NASA
Technical
Paper
3295

February 1993

Characterization and Durability Testing of Plasma-Sprayed Zirconia-Yttria and Hafnia-Yttria Thermal Barrier Coatings

Part I—Effect of Spray Parameters on the Performance of Several Lots of Partially Stabilized Zirconia-Yttria Powder

Robert A. Miller,
George W. Leissler,
and J. Marcus Jobe

NASA

NASA Technical Paper 3295

1993

Characterization and Durability Testing of Plasma-Sprayed Zirconia-Yttria and Hafnia-Yttria Thermal Barrier Coatings

Part I—Effect of Spray Parameters on the Performance of Several Lots of Partially Stabilized Zirconia-Yttria Powder

Robert A. Miller
Lewis Research Center
Cleveland, Ohio

George W. Leissler
Sverdrup Technology, Inc.
Brook Park, Ohio

J. Marcus Jobe
Miami University
Oxford, Ohio

NASA
National Aeronautics and Space Administration
Office of Management
Scientific and Technical Information Program

Summary

This and the following report discuss initial experiments conducted on thermal barrier coatings prepared in the newly upgraded research plasma spray facility and the burner rig test facilities. Part I discusses experiments which establish the spray parameters for three baseline zirconia-yttria coatings. The quality of five similar coating lots was judged primarily by their responses to burner rig exposure supplemented by data from other sources such as specimen characterizations and thermal diffusivity measurements. This study showed (after allowing for burner rig variability) that, although there appears to be an optimum density (i.e., optimum microstructure) for maximum burner rig life, the distribution tends to be rather broad about the maximum. In Part II, new hafnia-yttria-based coatings were evaluated against both baseline and alternate zirconia-yttria coatings. The hafnia-yttria coatings and the zirconia-yttria coatings that were prepared by an alternate powder vendor were very sensitive to plasma spray parameters in that high-quality coatings were only obtained when certain parameters were employed. The reasons for this important observation are not understood. Also not understood is that the first of two replicate specimens sprayed for Part I consistently performed better than the second specimen. In Part II, this spray order effect was not observed, possibly because a chiller was installed in the torch cooling water circuit. Also, large changes in coating density were observed after we switched to a new lot of electrodes. Analyses of these findings were made possible, in part, because of the development of a sensitive density measurement technique described herein in detail.

The measured thermal diffusivities did not display the expected strong relationship with porosity. This surprising result was believed to have been caused by increased microcracking of the denser coatings on the stainless steel substrates.

Introduction

This report discusses the initial investigations conducted after the plasma spray and burner rig test facilities at the NASA Lewis Research Center were upgraded. The equipment, personnel, and organizational structure are all different from those reported in most prior NASA Lewis publications. (One exception is the study reported by Brindley and Miller (1990) in that their work was started at the beginning of the transitional period.) Now in use in both atmospheric and low-pressure environments are new plasma spray torches that are robotically controlled rather than hand held. Closed-loop powder feeders, noncontact thickness monitoring, and pyrometric monitoring of specimen surface temperatures are now also used. A new burner rig laboratory and new approaches to testing are other changes.

As a result of the upgrading, especially changes involving automation and plasma spray torches, new operating procedures had to be devised. Thus, this report discusses the progress to date with respect to a variety of characterization methods, burner rig durability testing, and statistical error analysis. Suggestions are made for future work that will utilize what is learned about conducting effective thermal barrier coating (TBC) research in these new facilities. This study, in addressing the foregoing topics, raised as many questions as were answered.

Experimental Procedure

Five lots of zirconia-yttria (ZrO_2-Y_2O_3) powder were compared in this study. All were prepared by the same vendor and were similar in nominal composition: yttria was in the 6 to 9 wt% partially stabilized range.

Specimens for thermal diffusivity and density measurements were grit-blasted, flat stainless steel substrates, nominally 1.3 by 5.1 by 0.16 cm (0.5 by 2 by 0.06 in.) with ceramic sprayed to a thickness of approximately 0.05 cm (0.02 in.). The burner rig durability specimens were solid Waspaloy cylinders, 1.3 cm (0.5 in.) in diameter, coated over a 10-cm (4-in.) length with about 0.013 cm (0.005 in.) of low-pressure, plasma-sprayed −325 mesh nickel (Ni) −35% chromium (Cr) −5% aluminum (Al) −1% yttrium (Y) (or ytterbium (Yb)) bond coat. The cylinder was then coated with 0.025 cm (0.010 in.) of atmospheric pressure, plasma-sprayed zirconia-yttria ceramic.

The plasma spray torch used to prepare the ceramic coatings was an Electro-Plasma Incorporated (EPI) model 03CP plasma generator with a 03CA–027 cathode and a 03CA–167 anode. An external injection powder port was affixed to the torch. The powder was delivered through a closed-loop hopper. The power supply was two 40-kW

rectifiers. Gas flow rates were monitored by mass flow controllers. The robot was a computer-controlled, six-axis dc servo articulated arm.

The arc gas used to spray the ceramic coatings was argon (Ar) with either 20 or 40 percent helium (He) secondary arc gas. The total arc gas flow was 24 SLPM (standard liters per minute) or 51 SCFH (standard cubic feet per hour). The powder carrier gas was argon at flow rates between 1.5 and 6.0 SLPM (3.2 and 12.7 SCFH). Additional argon, with a flow rate equal to that of the powder carrier gas, was allowed to flow through an internal injection port in the nozzle. (This port is used for air plasma spraying of metals. The argon flow was intended to provide some cooling to the nozzle although its effectiveness was not studied.) The powder was injected externally at 15 or 20 g/min (0.033 or 0.044 lbm/min) to yield about 0.0025 cm (0.001 in.) of deposit per pass. The coating thickness was monitored by using a high-resolution video camera and width analyzer (Miller, 1988). The specimen surface temperature was monitored by using an infrared pyrometer. Cooling air was applied to the front surface of the specimens between each pass until the surface temperature dropped to 200 °C (400 °F). The traverse speed was 10.0 cm/sec (4.0 in./sec).

The bond coats were applied with an EPI 03CK, 120-kW plasma generator with a 03CA–82 cathode and a 03CA–132 anode modified to a 1.27-cm (0.5-in.) nozzle diameter. The primary arc gas was argon at 50 SLPM (105 SCFH), and the auxiliary arc gas was a mixture of argon-3.8% hydrogen (H_2) at 29 SLPM (62 SCFH). The powder carrier gas was argon at a flow rate of 10 SLPM (22 SCFH) and a powder feed rate of 59 g/min (0.13 lb/min). The power level for this portion of the study was 65 kW at 1300 A; the reverse transfer arc power was 1.5 kW; the tank pressure was 3800 Pa (28.5 torr); and the standoff distance was 40.9 cm (16.1 in.). The part was rotated at 60 rpm and the traverse speed was 152 cm/sec (60 in./sec).

The thermal diffusivities of selected specimens were measured by using the flash diffusivity technique. The heat capacity was measured by using differential scanning calorimetry (Taylor, 1982). These two properties plus the NASA-supplied densities were then used to calculate thermal conductivity.

Bulk densities were measured by the mercury Archimedes method, which is described in the appendix. The porosity was taken as 100 minus the percent of theoretical density. The theoretical density of the zirconia-yttria coating was taken as 5.73 g/cc (0.207 lbm/in.^{3}) (Van Roode and Beardsley, 1988). Roughnesses were measured with a commercial diamond stylus profilometer using a 0.08-cm (0.03-in.) cutoff (American National Standards Institute/American Society of Mechanical Engineers, 1986). Several specimens were also analyzed by x-ray diffraction, which was restricted to scans of the (111) and (400) regions to provide a semiquantitative phase analysis (Miller et al., 1981; Miller et al., 1983).

The two burner rigs, similar to those described by Hodge et al., 1978, burned JP5 jet fuel and 260 °C (500 °F) preheated air at a combustor pressure of 6890 Pa (1 psig). The exhaust gases exited the combustor through a nozzle and were accelerated to Mach 0.3. A rotating carousel with four coated, solid cylindrical specimens was placed a few centimeters from the nozzle for 6 min during the heating cycle.

Results and Discussion

Spray Powder Characterization

The five lots of zirconia-yttria powder compared in this portion of the study consisted of

(1) A1: prepared in 1985 according to NASA specifications
(2) A2: a 1988 off-the-shelf purchase
(3) A3: lot A2 with a portion of the fine particles removed by the vendor
(4) A4: lot A2 with coarse particles removed
(5) A5: a 1989 off-the-shelf sample

The goals of this portion of the study were to establish baseline coatings and to investigate the responses of five similar starting materials to processing and evaluation.

Chemistries and particle size distributions for the powder lots.—In this section the chemical and particle size analyses of the starting powders are reported. Both sets of measurements were performed at NASA and by the vendor.

Chemical analyses of lots A1 to A3 and A5: Table I gives the levels of zirconia, yttria, hafnia, and six trace impurities according to analyses done by both the vendor and analysts at the NASA Lewis Research Center. In the case of lot A2, the analysis was repeated at various times. The NASA analyses were usually done by x-ray fluorescence except where noted. All the NASA results represent the average of at least three replicates. (Precision among the three replicates tended to be excellent.) An inspection of the table reveals that the analyses of yttria by both NASA and the vendor and between NASA measurements on various dates was consistent. However, considerable variability in two of the minor constituents (iron oxide and silica) was noted. Whether this error is caused by the analysis, such as in the preparation of standards, or is the result of actual variations in the powder lots is presently unknown. It should be noted that standard procedures for selecting powder samples (Allen, 1974) were not followed and that this could have contributed to the observed variations.

Particle size distributions for lots A1 to A5: Table II gives the cumulative particle size distributions for lots A1 to A5. All lots, except A4, were measured at NASA Lewis by using standard sieves. The distribution for lot A4 was not measured but instead was estimated from the −200 portion of lot A2. All five lots had the majority of the

TABLE I.—CHEMICAL ANALYSIS BY X-RAY FLUORESCENCE SPECTROMETRY OF LOTS A1 TO A3 AND A5[a]

[Values obtained by NASA analyses represent the average of at least three replicates.]

Lot	Analysis	Composition, wt %								
		Zirconia	Yttria	Hafnia	Alumina	Calcia	Iron oxide	Silica	Titania	Magnesia
A1	Vendor	Bal	[b]6–1/2	----	0.02	0.14	0.06	0.09	0.06	0.02
	NASA (3/85)		6.79	1.81	[c].4	[c].1	[c].005	[c].43	[c].03	[c].01
A2	Vendor	Bal	8.34	1.65	0.06	0.19	0.15	0.20	0.06	0.05
	NASA (11/88)		8.44	1.74	.08	.22	.04	.19	.06	---
	NASA (1/81)		8.47	1.74	.02	.17	.12	.22	.07	---
	NASA (3/91)		8.44	1.72	.07	.20	.39	.40	---	---
	NASA (7/91)		8.37	1.81	.03	.18	.07	.38	.06	<.5
A3	Vendor	Bal	7.85	1.84	0.12	0.18	0.11	0.33	0.06	0.03
	NASA (7/91)		8.41	1.79	.03	.18	.07	.37	.06	<.5
A5	Vendor	Bal	7.78	1.69	0.09	0.019	.13	.23	.08	.02

[a]Lot A4 assumed to be the same as lot A2.
[b]As reported by the vendor.
[c]NASA analysis by flame atomic absorption spectrometry.

TABLE II.—CUMULATIVE PARTICLE SIZE DISTRIBUTION FOR LOTS A1 TO A5

Particle size range		Cumulative particle distribution, percent				
Sieve size	μm	Lot				
		A1	A2	A3	A4	A5
−325	−44	9.4	18.1	5.6	20.7	13.6
−270/+325	−53/+44	27.3	36.9	25.5	42.3	31.9
−230/+270	−62/+53	52.2	61.2	54.2	70.1	59.3
−200/+230	−74/+62	83.9	87.3	85.5	100.0	87.0
−170/+200	−88/+74	98.6	99.5	99.2	100.0	98.2
−140/170	−105/+88	99.3	99.9	99.8	100.0	99.7

powder in the range −200/+325 (−74/+44 μm) with between 0 and 0.7 wt% above 200 mesh and between 5.6 and 20.7 wt% below 325 mesh.

The sieve analyses at NASA compared well with the vendor-supplied analyses. Limited attempts to measure particle size distribution by the methods of electrical sensing zone and laser light scattering yielded distributions that were shifted to larger particle sizes. Thus, it may be advisable to use caution when comparing sieve analysis data to automated data.

TABLE III.—PROCESSING PARAMETERS AND SPECIMEN PROPERTIES

Lot	Parameter set[a]	Electrode set	Roughness,[b] Ra, μm (μin.)	Standard error, μm (μin.)	Density,[c] percent theoretical	Diffusivity measured	Percent monoclinic intensity	Thickness, cm (mil)	Deposition efficiency, percent
A1	45/20/3	2	10.4 (411)	0.41 (16)	90.2	---	---	0.016 (6.5)	8
	55/20/3		10.1 (399)	.30 (12)	95.0			.0325 (12.8)	17
	40/40/3		10.3 (407)	.51 (20)	95.0			.0396 (15.6)	28
	40/40/4		9.8 (384)	.20 (8)	95.7			.0427 (16.8)	32
	40/40/5		9.5 (373)	.36 (14)	95.8			.0411 (16.2)	31
A2	45/20/2	1	13.8 (542)	0.48 (19)	82.8			0.0373 (14.7)	20
	45/20/3		12.7 (501)	.46 (18)	84.4			.0513 (20.2)	31
	45/20/4		11.7 (460)	.38 (15)	86.1	Yes	1.4	.0465 (18.3)	23
	45/20/5		12.3 (486)	.30 (12)	87.9			.0452 (17.8)	23
	55/20/2		12.3 (486)	.51 (20)	89.9			.0508 (20.0)	35
	55/20/3		11.5 (451)	.46 (18)	91.0			.0518 (20.4)	38
	55/20/4		11.0 (433)	.30 (12)	90.9	Yes	1.1	.0444 (17.5)	28
	55/20/5		10.6 (417)	.51 (20)	90.2			.0376 (14.8)	24
	40/40/1.5		13.2 (520)	.66 (26)	86.2	Yes	1.6	.0526 (20.7)	34
	40/40/2.5		12.0 (471)	.58 (23)	86.3			.0478 (18.8)	31
	40/40/2.5		11.2 (439)	.51 (20)	88.3			.0483 (19.0)	32
	40/40/3		11.2 (441)	.48 (19)	88.4			.0503 (19.8)	34
	40/40/4		11.7 (461)	.46 (18)	89.6	Yes	1.6	.0523 (20.6)	39
	40/40/3	2	11.7 (460)	0.51 (20)	92.5			0.0521 (20.5)	38
	40/40/4		11.4 (448)	.41 (16)	94.0		1.7	.0508 (20.0)	36
	40/40/5		10.7 (420)	.43 (17)	93.6			.0605 (23.8)	49
	40/40/3		11.3 (445)	.48 (19)	92.3			.0622 (24.5)	47
	40/40/4		11.0 (434)	.30 (12)	93.4	Yes	1.2	.0541 (21.3)	43
	40/40/5		10.6 (416)	.33 (13)	93.3			.0566 (22.3)	42
	45/40/4		10.4 (409)	.28 (11)	94.7			.0594 (23.4)	49
	45/40/3		11.1 (438)	.38 (15)	93.7			.0508 (20.0)	35
	45/40/4		11.6 (456)	.36 (14)	94.0		1.4	.0660 (26.0)	55
	45/40/5		9.9 (388)	.33 (13)	93.4			.0592 (23.3)	47
A3	40/40/1.5	1	13.1 (514)	0.56 (22)	81.8			0.0429 (16.9)	25
	40/40/2		13.3 (524)	.36 (14)	82.6			.0498 (19.6)	34
	40/40/3		14.2 (559)	.51 (20)	86.7			.0523 (20.6)	37
	40/40/4		13.0 (512)	.79 (31)	89.0	Yes	1.4	.0518 (20.4)	36
	40/40/5		11.7 (461)	.56 (22)	89.4			.0523 (20.6)	41
	40/40/6		11.0 (433)	.56 (22)	90.0			.0447 (17.6)	34
A4	40/40/1.5	1	12.4 (490)	0.53 (22)	85.2	Yes	1.7	0.0457 (18.0)	29
	40/40/2		11.9 (470)	.46 (18)	85.4			.0488 (19.2)	32
	40/40/2.5		12.9 (506)	.61 (24)	87.9			.0508 (20.0)	36
	40/40/3		12.0 (472)	.56 (22)	89.8			.0508 (20.0)	34
	40/40/4		11.3 (443)	.53 (21)	90.6			.0513 (20.2)	36
A5	40/40/2.5	2	12.3 (485)	0.41 (16)	92.9			0.0483 (19.0)	35
	40/40/4		11.0 (434)	.48 (9)	93.0			.0478 (18.8)	34

[a]Set designation: (power level, kW)/(percent of He in Ar)/(powder carrier gas flow rate, SLPM (SCFH)).
[b]Average value of nine measurements per specimen.
[c]Average value of two specimens measured.

Initial parameter effect study.—Specimens for this portion of the study were grit-blasted, flat stainless steel substrates coated with a single layer of plasma-sprayed zirconia-yttria powder as described in **Experimental Procedure**. Table III lists processing parameters and various measured properties for these specimens.

Porosity/bulk density, surface roughness, and x-ray phase analysis: Values for porosity, roughness, and percent monoclinic intensity are given in table III. The 95-percent confidence intervals of these measurements, based on pooled standard deviations from multiple tests, were ±0.7 percent for the porosity based on 70 pairs of measurements; 0.91 μm (±36 μin.) for the roughness based on 40 pairs of measurements; and ±0.5 percent for the percent monoclinic intensity based on 10 pairs of measurements. The latter value is a strong function of the percent intensity and refers to

values for the range given in table III. The confidence interval indicates that repeated measurements would fall within that interval 95 percent of the time.

Figure 1(a) shows the relationship between density and powder carrier gas flow rate for five powders sprayed using an Ar-40% He arc gas (flow rate, 24 SLPM (51 SCFH)) at a 40-kW power level. Figure 1(b) shows density versus powder carrier gas flow rate for one powder lot at three different power levels and arc gas flow rates. Two different batches of electrodes are represented in these plots. The plots show a strong dependence between powder carrier gas flow rate and density with curves which appear to be smooth to within the 95-percent confidence interval for the density measurements (which were estimated to be ±0.7 percent). It is important to note that centerline injection (defined here as injection that places most of the powder along the center of the plasma flame) was observed at about 2.5 SLPM (5.3 SCFH). The denser coatings were obtained when the powder was injected past the centerline (away from the powder port) whereas the more porous coatings were obtained with injection less than the centerline (towards the powder port). In fact, centerline injection appears to be undesirable because the change in density with increasing powder gas flow rate is at a maximum at that point. The figure also shows the large systematic variation in density that was noted upon switching the anode and cathode from an old batch to a new one.

Figures 2(a) and (b) show schematically the particle trajectories expected for low and high powder carrier gas flow rates, respectively.

The figures show the powder particles exiting the powder port and entering the flame, which entrains them and carries them towards the target. The drawing indicates that the hottest portion of the flame extends comparatively far from the nozzle, which is characteristic of an Ar-40%He flame. Furthermore, the drawing is simplified in that turbulent mixing with the atmosphere is not indicated (i.e., it is based on fig. 2 from Boch et al., 1984 rather than on fig. 11 from Spores and Pfender, 1989). At the low powder carrier gas flow rate in figure 2(a), the heavier (coarser) particles are pushed into the flame only as far as the centerline whereas the lighter (finer) particles do not penetrate as far into or bounce off the viscous Ar-He flame. These conditions produce a less melted and more porous coating which deposits mostly above the centerline. At the high powder carrier gas flow rate in figure 2(b), the lighter particles are traveling along the centerline whereas the heavier particles are pushed further through the flame. These conditions produce more complete melting and shift most of the deposit to the opposite side of the centerline. Because a plasma containing zirconia glows with a characteristic yellow color when viewed, the trajectory with respect to the centerline is easily observed (through protective glasses). It should be mentioned that this approach is contrary to convention which favors centerline injection (Boch et al., 1984; Thorpe and Kratochvil, 1989, fig. 12).

Figures 3(a) and (b) show the relationship between powder gas flow rate and deposition efficiency. (Deposition efficiency is defined herein as the percentage by weight of the powder that deposits on the substrate during that portion of the time that the torch is aimed at the substrate.) Although there are potential sources of systematic error in this measurement, such as the effect of unnoticed changes in the flame orientation which may have caused the particles to partially miss the substrate, certain observations can be made from these plots. From figure 3(a), most of the results from lots A2 to A5 (which are similar lots) fell in a narrow band, and a small but not precipitous drop in deposition efficiency occurred with decreasing powder gas flow rate. For powder lot A1, the falloff may have been more severe. Also, for lots A2 to A5, the deposition efficiencies obtained by using the new batch of electrodes tended to exceed those obtained by using the old electrodes. Figure 3(b) indicates that the lower enthalpy (45kW), Ar-20% He flame may have caused a loss in deposition efficiency. Therefore, although lower enthalpy flames may be used to produce more porous coatings, there is a deposition efficiency penalty. On the other hand, using a high enthalpy flame with a low powder carrier gas flow rate produced a more porous coating without a significant loss in deposition efficiency.

Based on table III and figures 1 and 3, a powder carrier gas flow rate of about 4.5 SLPM (9.5 SCFH) was always at or near the peak density for a given power-arc gas combination whereas a SLPM of 1.5 to 2 (3.2 to 4.2 SCFH) gave a more porous coating while maintaining good deposition efficiency. This observation was considered when subsequent burner rig specimens were prepared.

The values of the surface roughness in table III are the averages of nine measurements per specimen. There was considerable scatter in these measurements (as reported earlier in this section, the 95-percent confidence interval for the average of nine measurements is ±0.91 μm (±36 μin.)); this variation appeared to have been an indication of the actual variations in the surface texture rather than a measurement error. If these mean roughness values are plotted against the measured porosity (fig.4), there appears to be a correlation between these two parameters, which was expected because both properties are related to particle melting. Regressing the roughness against the porosity gives the solid line in the figure. (Roughness was treated as the dependent variable for this regression because the relative standard deviation for the roughness measurement is greater for roughness than the relative standard deviation for the porosity measurement, and conventional regression techniques assume that only the dependent variable has error.) The dotted lines represent the 95-percent confidence interval and the dashed lines the 95-percent prediction interval. Although the confidence intervals are spaced narrowly apart (because of the relatively large number of points), the wide spacing of the prediction interval lines

TABLE IV.—MEASURED 200 °C (400 °F) THERMAL DIFFUSIVITIES α AND THERMAL CONDUCTIVITIES *k* AND ADDITIONAL PERTINENT SPECIMEN DATA

Lot	Parameter set[a]	Electrode set	Substrate thickness,[b] cm (mil)	Ceramic thickness,[c] cm (mil)	Porosity percent	Thermal conductivity, *k*, W/m-°C	Thermal diffusivity, α, cm^2/sec
A2	45/20/4	1	0.1518 (59.8)	0.0470 (18.5)	14.0	0.97	0.00364
	40/40/1.5	1	.1483 (58.4)	.0528 (20.8)	13.8	1.12	.00414
	40/40/4	1	.1481 (58.3)	.0528 (20.8)	10.3	1.13	.00409
	40/40/4	2	.1499 (59.0)	.0554 (21.8)	6.6	.93	.00318
	45/40/4	2	.1529 (60.2)	.0599 (23.6)	5.2	1.01	.00361
A3	40/40/4	1	0.1509 (59.4)	.0518 (20.4)	11.0	1.05	0.00375
A4	40/40/4	1	0.1483 (58.4)	0.0521 (20.5)	9.4	1.24	0.00444
	40/40/1.5	1	.1478 (58.2)	.0462 (18.2)	14.9	1.32	.00499

[a]Set designation: (power level, kW)/(percent of He in Ar)/(powder carrier gas flow rate, SLPM).
[b]Value measured for the actual specimen being analyzed.
[c]Value attained after the coating was smoothed to ~ 4 μm (~100 μin.) with SiC paper.

indicates that the errors in the measurement of roughness preclude the possibility of using roughness as a measure of porosity. However, it is possible that another roughness measurement approach, such as an optical technique, may be able to rapidly measure roughness over a wide area with a lower standard deviation. If so, such a technique could possibly provide an indication of the porosity from surface roughness.

Figure 5 presents the percent theoretical density versus the deposition efficiency (fig. 5(a)) and the percent monoclinic intensity (fig. 5(b)). Figure 5(a) shows a positive correlation and figure 5(b) shows what appears to be a negative correlation. These trends were anticipated because more complete melting leads to higher density, higher deposition efficiency, and a lower percentage of the monoclinic phase. However, the scatter is too great to make practical use of either of these plots.

Figure 6 is a typical x-ray diffraction pattern from the (400) region. These plots indicate that the plasma-sprayed coatings are primarily the tetragonal phase (believed to be the t′-nontransformable tetragonal phase) plus, possibly, small amounts of the cubic phase. The t′-phase is believed to be quite stable at temperatures below about 1200 °C (2190 °F) (Miller et al., 1981).

Thermal diffusivities, heat capacities, and thermal conductivities: The specimens selected for the thermal diffusivity measurements are noted in table III. Additional information is given in table IV. All specimens noted in this table were measured while they were attached to approximately 0.15-cm- (0.060-in.-) thick stainless steel substrates. (As will be discussed later, this choice of substrate material is believed to have affected the coating microstructure and properties.) Thermal diffusivities of the coating-substrate combinations and of the substrate alone were measured from room temperature to 1200 °C (2190 °F) and then back again to room temperature. Heat capacities C_p were measured from room temperature to 600 °C (1110 °F) and were then extrapolated by the contractor to higher temperatures. The thickness is the value attained after the coating was smoothed to about 4 μm (100 μin.) by using SiC paper. The porosities noted in table IV refer to the values measured for the actual specimens being analyzed whereas the values in table III are the average of two specimens.

Figure 7(a) shows the heat capacities measured for the eight zirconia-yttria specimens, and figure 7(b) shows a regression fit with the associated 95-percent confidence intervals. The responses for all the specimens were similar, which was not surprising because all eight of these coatings were prepared from the closely related lots A2 to A4. They differed only by structure, which should have a minimal effect on the heat capacity. However, note that the curves begin to diverge at temperatures between 400 and 600 °C (750 and 1110 °F). If this divergence were to be reflected in the extrapolated heat capacities, a systematic error may be introduced in the conversion from thermal diffusivity to thermal conductivity at high temperatures.

The effects of heating and cooling on the measured thermal diffusivities are shown in figures 8(a) and (b), respectively. Note that in figure 8(a) the measured diffusivities generally decrease between 23 and 800 °C (73 and 1470 °F) although the behavior between 23 and 100 °C (73 and 210 °F) is erratic. The curves then level off between 800 and 1200 °C (1470 and 2190 °F). On cooling (fig. 8(b)), the values tend to decrease between 1200 and 800 °C (2190 and 1470 °F) and generally increase between 800 °C (1470 °F) and room temperature. Thermal conductivities *k* are plotted in figures 9(a) and (b). The contractor calculated these values by using $k = \alpha C_p \rho$, the contractor-measured diffusivities α, the contractor-measured and extrapolated heat capacities C_p, and the NASA-measured densities. On first heating (fig. 9(a)), the thermal conductivities tended to rise to a maximum value at 200 °C (400 °F), to fall rather

rapidly at 400 °C (750 °F), and to level off at intermediate temperatures until they rose somewhat at higher temperatures. On cooling (fig. 9(b)), the conductivities tended to drop at 1200 to about 700 °C (2190 to 1290 °F) and were fairly level until 200 °C (400 °F). Below 200 °C (400 °F), the behavior was erratic. The hump observed at 200 °C (400 °F) on heating was not evident on cooling.

The most striking feature of the plots in figures 8 and 9 is that the expected sharp decrease in conductivity and diffusivity with increasing porosity is not apparent, nor is it apparent in figures 10(a) and (b) where the 200 °C (400 °F) thermal diffusivities (a) and the 200 °C (400 °F) thermal conductivities measured both on heating and cooling (b) are plotted against the percent porosity.

An inspection of figures 8 to 10 not only fails to show the sharply downward trend expected but instead reveals that it appears to be slightly upward although the scatter in the data prevents statistical confirmation of this hypothesis.

Figure 11 provides a probable explanation for the apparent discrepancy just discussed. Figure 11 (top) is a photomicrograph of one of the denser coatings, and figure 11 (bottom) is a photomicrograph of one of the more porous coatings. These photomicrographs were carefully prepared by a process that includes vacuum infiltration of the epoxy mounting media (Brindley and Leonhardt, 1990). These figures show that, although there are many pores in the more porous coating, more microcracking occurred in the denser coating and the microcracks were wider. Microcracking is known to lower thermal conductivity (Hasselman, 1978); therefore, it is possible for the thermal resistance of the denser more microcracked coatings to be comparable to the resistance of porous coatings.

The high thermal expansion of stainless steel at low temperatures may have had a strong influence on the amount of microcracking observed in these specimens. For example, the mean coefficient of thermal expansion (CTE) for 304 stainless steel from 0 to 100 °C (32 to 210 °F) is 17 μm/m-°C (9 μin./in.-°F) (Metals Handbook, 1987) compared to about 12 μm/m-°C (7 μin./in.-°F) from room temperature to 100 °C (210 °F) for typical superalloys and bond coats (DiMasi et al, 1989; High Temperature-High Strength Nickel Base Alloys, 1984). Since the CTE value for the zirconia-yttria layer is about 10 μm/m-°C (6 μin./in.-°F) (DiMasi et al., 1989), the difference in CTE at 100 °C (210 °F) between a zirconia-yttria coating and a stainless steel substrate is 3.5 times larger than the difference for the same coating on a superalloy substrate.

Microcracking, as influenced by the thermal expansion mismatch stresses between the stainless steel substrate and the ceramic, may also explain the general features of figures 8 and 9. If one assumes that the "stress-free temperature" (Sevcik and Stoner, 1978) is a few hundred degrees centigrade in the as-sprayed coating, then the thermal expansion mismatch stresses will be minimal at that temperature. This condition could have led to a minimum in the extent of cracking at the stress-free temperature and therefore may explain the maximum in the thermal conductivities observed at about 200 °C (400 °F). When the specimen is heated to 1200 °C (2190 °F), the stress-free temperature should increase to that temperature because of the relaxation of the substrate, but on gradual cooling the stress-free temperature should drop again until the yield stress of the substrate becomes sufficiently large to prevent further decrease. At that point the conductivities should begin to rise upon further cooling. The heating-cooling cycle should lead to wider microcracking and result in lower conductivities.

The thermal diffusivity of two of these specimens was remeasured after the ceramic was removed from the substrate (by heating in hydrochloric acid). One ceramic was the most dense and the other was one of the more porous. In both cases, the measured value increased by 15 percent so that the diffusivity of the more porous ceramic still exceeded that of the more dense ceramic. This result was not surprising because the microcrack network set up while the ceramic was attached to the substrate remained after its removal. The higher diffusivities measured after the removal could have resulted from a decrease in the crack displacement after the ceramic was removed from the substrate; however, the magnitude of the effect is probably within experimental error.

Durability of thermal barrier coating systems prepared from zirconia-yttria lots A1 to A5.—This portion of the report describes the characterization and durability testing of zirconia-yttria thermal-barrier-coated test specimens. These specimens were cyclindical superalloy substrates with a thin thermal-barrier-coating system. This system consisted of a layer of low-pressure, plasma-sprayed metallic bond coat and a layer of atmospheric pressure, plasma-sprayed zirconia-yttria ceramic, with starting materials and spray parameters selected from the section ***Chemistries and particle size distributions for the powder lots.*** Companion specimens of the type described in this section were also prepared immediately before or immediately after the preparation of each set of durability specimens. These companion specimens were used to obtain measurements of the density and other properties of the coating.

Preparation of durability specimen: The coated cylindrical test specimens were prepared by using the materials and equipment discussed in the **Experimental Procedure** section; the parameters were selected from the section ***Initial parameter effect study***. Four sets of parameters were selected and are designated 40/40/4.5, 55/20/4.5, 45/20/4.5, and 45/20/1.5, which designations refer to the power level in kilowatts; the percent of He in Ar; and the powder carrier gas flow rate in SLPM, respectively. The first three sets were used to spray all five lots of powder. The fourth set was only used for lot A2. The specimens were rotated at 360 rpm, and the traverse speed was 1.0 cm/sec (0.4in./sec); thus, the narrow, atmospheric

TABLE V.—ZIRCONIA-YTTRIA DURABILITY TEST DATA

Nominal powder composition	Lot	Parameter set[a]	Roughness, Ra, μm (μin.)	Density, percent	Order	Test life, cycles	
						Rig 1	Rig 2
$ZrO_2-7Y_2O_3$	A1	40/20/4.5	10.8 (424)	----	–	138	----
					–	----	106
		45/20/4.5	11.0 (432)	94.5	1	394	----
					2	----	246
		55/20/4.5	10.1 (397)	95.7	1	----	213
					2	374	----
		40/40/4.5	9.3 (366)	96.7	1	----	410
					2	509	----
$ZrO_2-8Y_2O_3$	A2	40/40/1.5	14.3 (563)	90.2	1	----	957
					2	----	553
		45/20/4.5	13.2 (518)	88.0	1	----	477
					2	----	475
		55/20/4.5	11.1 (438)	94.4	1	----	831
					2	----	576
		40/40/4.5	11.4 (447)	96.1	1	----	743
					2	----	466
	A3	45/20/4.5	12.2 (482)	87.6	1	----	823
					2	1003	----
		55/20/4.5	12.5 (494)	92.4	1	----	887
					2	1096	----
		40/40/4.5	12.6 (497)	93.6	1	----	799
					2	1215	----
	A4	45/20/4.5	11.9 (470)	90.2	1	----	975
					2	----	542
		55/20/4.5	11.2 (441)	94.5	1	----	687
					2	873	----
		40/40/4.5	11.7 (461)	94.6	1	----	911
					2	1057	----
	A5	45/20/4.5	13.2 (518)	89.7	1	----	1174
					2	1197	----
		55/20/4.5	13.5 (530)	90.0	1	----	1112
					2	1214	----
		40/40/4.5	11.3 (446)	95.0	1	----	883
					2	----	599

[a]Set designation: (power level, kW)/(percent of He in Ar)/(powder carrier gas flow rate, SLPM).

pressure, plasma-sprayed plume effectively traversed the specimen at 25 cm/sec (10 in./sec). The zirconia powder was fed in by using a closed-loop powder hopper typically at 15 g/min (0.33 lbm/min) so as to maintain about a 0.0025-cm (0.001-in.) deposit thickness per pass. The Waspaloy specimens were not pre-heated prior to the plasma spray deposition of the ceramic.

Two cylindrical specimens and two companion specimens of the type described in the section ***Initial parameter effect study*** were prepared for each parameter set. All bond coats and all ceramic layers were sprayed on consecutive days in the two rigs.

Density/porosity, roughness for companion coupons of the burner rig specimens: The companion specimens were approximately 1.3- by 5.1- by 0.16-cm (0.5- by 2- by 0.06-in.) stainless steel coupons which were grit blasted on one side and coated two at a time immediately before or immediately after the durability specimens were prepared. The results of these measurements are included in table V.

Burner Rig Durability Study

Brief description of burner rig test.—The specimens were tested in the four-specimen carousel shown in figure 12. Figure 13 shows the surface response of the coated specimens as measured by an infrared pyrometer. The effective time at maximum temperature for each cycle was 4.0 min. During testing, the specimen temperatures were read using a disappearing-filament pyrometer that was calibrated against a thermocouple spindle specimen. The

spindle specimen was a cylinder with a 1.3-cm (0.5-in.) diameter in the hot zone region and a 0.3-cm (0.12-in.) diameter outside the hot zone. The thermocouple was placed in a 0.13-cm- (0.053-in.-) diameter longitudinal well just under the surface of the wide portion of the specimen. The rotating spindle specimen was heated to the desired temperature in the burner rig flame, and its temperature was read with the disappearing-filament pyrometer. The pyrometer was aimed at a point that was about 60° downstream from the burner rig, which prevents interference due to reflections from the hot rig. In the actual test specimen, the diameter was constant over the entire length; therefore, there could be a small gradient across the thermal barrier coating system. No attempt was made to experimentally determine whether or not there was a small gradient because experimental confirmation would have been quite difficult.

Failure was considered to be the first indication of spalling or blistering with a rupture of the ceramic.

Durability test results.—The durability test results for the zirconia-yttria/Ni-35%Cr-5%Al-1%Y specimens are given in table V. For most lots, specimens were prepared by using three sets of parameters, which led to three structures, or three "densities." (The use of the term density to express structure is, of course, an oversimplification. However, precisely measured densities supported by high-quality photomicrographs can be used to reliably and quantitatively represent the coating structure.) The shorthand notation described in the section *Preparation of durability specimen* is used to identify the different sets of parameters in table V. For example, the notation 40/40/4.5 refers to 40-kW power, Ar-40%He arc gas, and 4.5 SLPM (9.5 SCFH) powder carrier gas rate.

Test lives are given in the last two columns of table V. These columns indicate in which of two burner rigs each specimen was tested. Test lives are the number of cycles until the ceramic layer spalled or at least blistered and cracked. Failure morphologies were similar to those described in Brindley and Miller (1990) for the ZrO_2-8%Y_2O_3/Ni-35%Cr-5%Al-1%Y durability test specimens. That is, failure occurred by delamination in the ceramic at or near the interface with the bond coat. The Order column indicates whether the specimen is the first or second sprayed of the two replicates.

An inspection of table V reveals that there were 11 cases in which one specimen was tested in rig 1 whereas its replicate was tested in rig 2. In all 11 cases, the specimen tested in rig 1 lasted longer than the one tested in rig 2. For a random process, the probability that one or the other rig would yield longer test lives in 11 out of 11 cases is 1 in 2^{11-1} or 0.1 percent. Therefore, a systematic trend was suspected. In six other cases, replicates were tested in the same rig. In all six cases, the specimen prepared first lasted longer than the specimen prepared second (although in one case they were nearly equal). This result again suggested a systematic trend due to an unplanned variable.

In figure 14(a), the burner rig lives of specimens from lots A2 to A5 are plotted (without regard to rig or spray order) against the density that was measured on the companion coupons. Only lots A2 to A5 are included because these spray powders were very similar and were all expected to respond similarly to the planned and unplanned variables. However no conclusions about the effects of the variables lot and density can be drawn from figure 14(a). The effects of the variables began to emerge when the same data were replotted in figures 14(b) and (c). In figure 14(b), only the second specimen sprayed was plotted; the results obtained for specimens tested in rig 1 were plotted with a solid symbol whereas those obtained for specimens tested in rig 2 were plotted with open symbols. Now each set of points is seen to reside in a narrow band with a possible maximum near the mean density. In figure 14(c), the rig 2 test life of the first specimen sprayed for each of the specimens from lot A2 to A5 was plotted against density. Fortunately, this plot included a specimen from each parameter set. The plot again showed a rather narrow band of responses with a possible maximum in life near the center of the density range. The single point in parenthesis represents the one specimen from spray order 1 whose test life was not appreciably longer than the specimen from spray order 2, both having been tested in the same rig.

An inspection of figures 14(b) and (c) provides important insights into the effects of the unplanned variables (rig and spray order) and the planned variables (density and lot).

Statistical analysis of the zirconia-yttria burner rig data.—Although the effects of spray order and test rig complicated the interpretation of the data in table V, it was still possible to statistically analyze the data in a manner that provided estimates of the effects of lot, density, and rig. First, in the same manner that figure 14(a) was broken into figures 14(b) and (c), the data were divided into two groups according to spray order.

In the first case (as seen in fig. 14(b)), the data were treated as a randomized block plan with missing data having the variables lot and rig and the covariables density and the square of density. The density terms were treated as covariates because they could not be precisely controlled. (It should be mentioned that the use of covariates is very common in the social sciences but less common though not unknown in engineering (Mason et al., 1989).) The conventional assumption employed was that the effect of the covariates was the same for each of the lots. Lot A1 was not included in the analysis because its covariate effect appeared to be different from the others. The dependent variable for this analysis was the log of the coating life. The log transformation improved the distribution of the residuals and generally improved the fit. The relatively high values of the F-statistic and the corresponding low values of the probability p are evidence that the effects of rig, density, and density squared are statistically significant at the $p < 0.05$ level. The difference between the mean log

of the lives of specimens in the two rigs was 0.274 with a 95-percent least significant interval (Mason et al., 1989) of ±0.071. This difference corresponds to an increase in life of 1.9 times in rig 1 over rig 2. The difference between the four lots of material was not significant at the $p < 0.05$ level but was significant at a more relaxed $p < 0.10$ level. Figure 15(a) shows on a linear scale the means for the four lots and the 95-percent confidence intervals obtained from the analysis after the rig variable and density covariates were accounted for.

In the second case (as seen in fig. 14(c)), the data corresponding to spray order 1 and rig 2 were analyzed. For this analysis, the one suspicious point at lot A2 (88 percent density, 477 cycles) was discarded. This is the only point representing the first specimen sprayed that did not survive significantly longer than the second one sprayed, even though both were tested in the same rig. The one independent variable for this analysis was the lot whereas the density and the density squared were the covariates. As discussed above, the lot effect was not significant at the $p < 0.05$ level although p is less than 0.10. The probabilities associated with the density covariates were each about 0.10. In fact, a better fit was obtained for a single linear covariate because of the preponderance of data at higher densities. Nevertheless, the squared term was retained because of expectations based on historical precedents (Stecura, 1985). Figure15(b) shows the means and confidence intervals for the four lots.

Photomicrographs of specimens from lot A2.—Figures 16(a) to (f) present photomicrographs of six of the eight specimens from lot A2. Shown are sections taken from near the base of the test specimens for the as-sprayed microstructure and in the hot zone of specimens after failure. For the as-sprayed microstructure sections, the ceramic was thin because the thickness of this layer was tapered from near the hot zone to each end. The sections from the hot zone after failure had features similar to those reported previously (Miller and Leissler, 1992; Brindley and Miller, 1990; DiMasi et al., 1989). The bond coat layers of the as-sprayed specimens were relatively dense although not free of porosity. This porosity coarsens and was observed primarily at the interface after testing. (The specimen in fig. 16(d), as-sprayed, was an exception in that it appeared to have been exposed to an elevated temperature.) After the test, a thin, thermally grown oxide layer was observed at the ceramic-bond coat interface in the hot zone with occasional stringers into the bond coat. This layer was expected to be alumina for this bond coat alloy; the precipitates in the bond coat after exposure are α-Cr (Brindley and Miller, 1990). A chromium depletion zone was apparent near the interface with the substrate but not at the interface with the oxide. The zirconia-yttria layer was rather porous, exhibiting a variety of pore sizes and microcracks. The as-sprayed structure for the denser specimen in figure 16(f, top) appeared to have fewer pores than the other as-sprayed micrographs. The correlation between measured porosity and appearance was more difficult to judge in the other micrographs of figure 16. The failure morphology was typical of other high-quality, plasma-sprayed thermal barrier coatings where failure occurs by delamination within the zirconia-yttria ceramic layer near the interface with the bond coat. Any difference between the first and second specimens sprayed was not apparent.

Summary of Results

High-precision (i.e., low random error) density measurements may be made by using the Archimedes method. The measurements should be made on coupons that are similar to the specimen substrate and are prepared at approximately the same time as the test specimens. Such measurements may be used as an aid to optimization, as a daily quality control check, and as a guide to make frequent adjustments to the spray parameters. Because surface roughness causes a large systematic error, an empirical correction may be applied to correct for this error although performing the density measurements in a soft vacuum would be preferable.

Varying the powder gas flow rate proved to be an effective way to manipulate the density. Low flow rates which caused the powder to remain above the centerline produced less dense coatings, especially if the finer particles were removed from the starting powder. High flow rates for injection past the centerline yielded the densest coatings. Centerline injection was not preferred because that condition caused the greatest uncertainty in coating density.

There appeared to be a relationship between density/porosity and roughness. This relationship could possibly be employed for routine quality control but would only be practical if a rapid and precise surface roughness measurement method could be used (e.g., an optical approach). The deposition efficiency was proportional to the density, and the percent monoclinic intensity in the as-sprayed, partially stabilized zirconia was inversely proportional to the density. However, considerable scatter was associated with these two relationships.

Using infrared pyrometry to monitor the surface temperature during deposition was an effective way to manage the residual stress during processing. Video thickness monitoring during plasma spray deposition was an effective way to measure the thickness of both cylindrical burner rig specimens and flat density specimens.

A four-specimen burner rig rotating carousel, in conjunction with video monitoring, worked well to identify the cycle during which spalling occurred. Solid specimens of a low-cost superalloy (such as Waspaloy) were acceptable substrates for this type of study. Considerable rig-to-rig variability was noted. Also, with this data, the first specimen prepared consistently outperformed the second.

Modifying the spray powder by sieving did not noticeably effect the coating performance after allowing for

density differences. Also, the effect of ceramic layer density (spray parameter) variations on the thermal-barrier-coating system life for the specimens prepared from the various powders provided by the same vendor for Part I was relatively minor over the range of densities investigated. However, as will be discussed in Part II, the effects of ceramic layer density and the spray parameter variations were major for powders prepared by another vendor. This result was the same for both a zirconia-yttria powder that was prepared in accordance with an engine company's specifications and for hafnia-yttria powders that were prepared to NASA specifications. The reason for this difference is not apparent; there is no obvious correlation between particle size distribution or chemistry.

Lots of zirconia-yttria recently obtained from the vendor have a much lower percentage of the monoclinic phase in both the starting powder and the as-sprayed powder than older lots such as A1. The newer lots are possibly more homogeneous "alloys." Also, the burner rig lives of the newer lots were longer than those of the older lot.

The following observations were made from the measurements of thermophysical properties of the specimens:

(1) The heat capacity curves for the eight similar zirconia-yttria thermal barrier coatings agreed well but the values extrapolated beyond 600 °C (1110 °F) may deviate, which would affect the calculations to convert thermal diffusivity to thermal conductivity.

(2) Thermal diffusivity and, to a somewhat lesser extent, thermal conductivity tended to increase with increasing porosity. This result was unexpected and believed to have been caused by increased in-plane microcracking in the denser coatings (the stainless steel substrate may have influenced the amount of microcracking because of its relatively high thermal expansion at lower temperatures).

(3) A maximum in the thermal conductivity curves was observed at 200 °C (400 °F) on heating. The conductivity fell off at higher temperatures until about 500 °C (930 °F). The thermal diffusivity curves also fell off above the maximum which tended to occur at room temperature or 100 °C (210 °F). Upon cooling, the thermal conductivity curves fell off rapidly from the maximum at 1200 °C (2190 °F) down to about 800 °C (1470 °F), then gradually rose until 200 °C (400 °F). The response below 200 °C (400 °F) was variable. Similar behavior upon cooling was observed with the thermal diffusivity plots. These curves may have been influenced by the $\Delta\alpha\Delta T$ stress. For both thermal diffusivity and conductivity, the cooling curves were displaced towards lower values, which was probably caused by delamination cracking near the ceramic-stainless steel interface.

Conclusions

The commercial plasma spray powder routinely used at the NASA Lewis Research Center appears to be an acceptable reference baseline material based on its performance in burner rigs and on its relative insensitivity to spray parameter variations. However, the use of other types of zirconia-yttria powders as a baseline material is not precluded.

Making ceramic layer density measurements on specimens prepared simultaneously with the test specimens is a useful technique for characterizing coatings under development and for quality control. The technique is precise and fairly rapid and may be used, for example, to monitor electrode degradation and the effect of electrode replacement. In fact, it may be advisable to alter spray parameters to adjust for such variations. These physical measurements should be supplemented by frequent carefully prepared metallographic cross sections.

Adjusting the feed gas flow rate is an effective way to control the bulk density of the coating, and it would lend itself well to density grading.

The thermal diffusivity/thermal conductivity may be strongly influenced by the choice of substrate. Substrates with higher thermal expansions may cause more microcracking, which leads to lower than expected diffusivity/conductivity for dense coatings.

Finally, these experiments demonstrated the value of using statistical analysis to quantify experimental results that will be used in decision making. Also demonstrated is the importance of conducting designed experiments to eliminate undesired effects such as rig-to-rig and carousel-to-carousel variability.

Lewis Research Center
National Aeronautics and Space Administration
Cleveland, Ohio
September 10, 1992

Appendix – Archimedes Bulk Density Measurements

This appendix describes a relatively quick and precise method for measuring the bulk density of plasma-sprayed ceramic coatings. The method is fast enough to be used as a routine inspection technique and precise enough to perform measurements on coatings that are attached to the substrate.

Although many approaches are available for making bulk density measurements, it is difficult to precisely measure bulk density on thin coatings (Van Roode and Beardsley, 1988). For this study, we selected the Archimedes method which determines the buoyancy of a specimen that is entirely immersed in mercury.

Figure 17 schematically shows the porosity measurement apparatus. The coated specimen in the figure is an approximately 1.3- by 5.1- by 0.16-cm- (0.5- by 2- by 0.06-in.-) stainless steel substrate coated with at least 0.05 cm (0.020 in.) of the ceramic. The substrate is grit blasted on one side, weighed to the nearest milligram prior to the coating application, and then weighed again after the coating application. A bond coat is not used. A thin push rod is then glued to the specimen by using cyanoacrylate. Mercury is placed in a 3.8-cm- (1.5-in.-) diameter container to a depth of at least 7.5 cm (3 in.). The container plus the mercury (weighing about 1.2 kg (2.61 lbm)) is placed on a high-tare-capacity balance that is able to measure to an accuracy of ±0.01 g (0.00035 oz). The push rod and the attached specimen are then attached to a rigid support. In the apparatus of figure 16, the support is simply a thin metal tube inserted in a rubber stopper, which in turn sits in a hole drilled in a metal plate. A bend in the push rod allows the tube to support the push-rod-specimen assemblage.

Because the rod is rigidly supported from above, the upward force due to the buoyancy is transmitted to the tared balance. The contribution to the buoyancy from the push rod is measured by inserting the rod a fixed distance into the mercury while it is attached to the substrate and then removing it from the substrate and inserting it to the same depth. Subtracting the second reading from the first gives the buoyancy of the specimen only.

The density of the mercury is obtained from standard tables. Alternatively, the following expression fits the standard values near room temperature:

$$\rho_{Hg} = 13.5952 - 0.002450\ T$$

where ρ_{Hg} is the density in grams per cubic centimeter of mercury at temperature in Celsius.

The overall (or total) density of the substrate plus the ceramic is

$$\rho_T = (B_T - B_{PR})/\rho_{Hg}$$

where ρ_T is the overall density in grams per cubic centimeter, B_T is the buoyancy of the substrate, ceramic, and the immersed portion of the push rod, and B_{PR} is the buoyancy of the push rod. Both buoyancy terms are in grams.

The density of the ceramic is found by considering that the total volume V_T equals the sum of the substrate and ceramic volumes:

$$V_T = V_S + V_C$$

or

$$(M/\rho)_T = (M/\rho)_S + (M/\rho)_C$$

where M is the mass in grams of the total system, the substrate, and the ceramic, respectively. Therefore, if the density of the substrate has been measured independently, then the ceramic density may be calculated from the measured substrate mass, the total mass, the buoyancy of the specimen plus the push rod, the buoyancy of the push rod alone, and the temperature of the mercury.

Unfortunately there is a significant systematic error in the value of the ceramic layer density measured by this technique unless the measurement is performed in a soft vacuum. The error is attributed to the air that is trapped in the surface roughness of the ceramic (see fig. VII-8 in Adamson, 1976). The measurements discussed herein were not conducted in a vacuum and therefore an empirical correction based on the measured surface roughness was applied. This correction factor was obtained by measuring the values of ρ_C for coatings of varying thicknesses on the standard stainless steel substrates. If one assumes that the structure does not change with thickness, then the plot of the reciprocal of the uncorrected density versus the roughness leads to a correction factor of the form

$$\rho_C[\ell/(\ell - \beta\ Ra)]\rho_{C,\text{UNCORRECTED}}$$

where ℓ is the thickness of the ceramic layer, β is an empirical constant, and Ra is the surface roughness. If ℓ and β are expressed in the same units, then the value of β is between about 1.5 and 2.0. The value 1.5 was used for the study reported herein.

References

Adamson, A.W.: Physical Chemistry of Surfaces. Third ed., John Wiley and Sons, 1976, pg. 347.

Allen, T.: Particle Size Measurement. Second ed., John Wiley and Sons, New York, 1974 pp. 13–29.

American National Standards Institute/American Society of Mechanical Engineers. ANSI/ASME B46.–1–1985. Surface Texture, 1985, pp.13–15.

Boch, P., et al.: Plasma-Sprayed Zirconia Coatings. International Conference on the Science and Technology of Zirconia II (Advances in Ceramics, Vol. 12), N. Claussen, M. Ruhle, and A.H. Hever, eds., American Ceramic Society, Columbus, OH, 1984, pp. 488–502.

Brindley, W.J.; and Leonhardt, T.A.: Metallographic Techniques for Evaluation of Thermal Barrier Coatings. Mater. Charact., vol. 24, no. 2, 1990, pp. 93–101.

Brindley, W.J.; and Miller, R.A.: Thermal Barrier Coating Life and Isothermal Oxidation of Low-Pressure Plasma-Sprayed Bond Coatings. Surf. Coat. Technol., vol. 43/44, no. 1–3, 1990, pp. 446–457.

Corrosion-Resistant Materials. Table 12: Typical Physical Properties of Wrought Stainless Steels, Annealed Condition. Metals Handbook, Ninth ed., Vol. 3: Properties and Selection, Metals Park, OH, 1987, pp. 34–35.

DiMasi, J.T.; Sheffler, K.D.; and Ortiz, M.: Thermal Barrier Coating Life Prediction Model Development, Phase I. (PWA–5970–40; Pratt and Whitney Aircraft Group; NASA Contract NAS3–23944) NASA CR–182230, 1989.

Hasselman, D.P.H.: Effect of Cracks on Thermal Conductivity. J. Compos. Mater., vol. 12, Oct. 1978, pp. 403–407.

High Temperature-High Strength Nickel Base Alloys. Internal Report. International Nickel Company, Saddle Brook, NJ, 1984.

Hodge, P.E., et al.: Thermal Barrier Coatings: Burner Rig Hot Corrosion Test Results. NASA TM–79005, 1978.

Mason, R.L.; Gunst, R.F.; and Hess, J.L.: Statistical Design and Analysis of Experiments: With Applications to Engineering Science. John Wiley and Sons, New York, 1989.

Miller, R.A.: High Resolution Video Monitoring of Coating Thickness During Plasma Spraying. Thermal Spray: Proceedings of the National Thermal Spray Conference, ASM International, Metals Park, OH, 1989, pp. 363–366. (Also NASA TM–101423, 1988).

Miller, R.A.; Garlick, R.G.; and Smialek, J.L.: Phase Distributions in Plasma-Sprayed Zirconia-Yttria. Am. Ceram. Soc. Bull., vol 62, no.12, 1983, pp. 1355–1358.

Miller, R.A.; and Leissler, G.W.: Characterization and Durability Testing of Several Plasma Sprayed Zirconia-Yttria and Hafnia-Yttria Thermal Barrier Coatings; Part II. Effect of Spray Parameters on the Performance of Four Lots of Hafnia-Yttria and Two Lots of Zirconia-Yttria. To be published as NASA TP–3296, 1992.

Miller, R.A.; Smialek, J.L.; and Garlick, R.G.: Phase Stability in Plasma-Sprayed, Partially Stabilized Zirconia-Yttria. Science and Technology of Zirconia; Proceedings of the First International Conference on the Science and Technology of Zirconia (Advances in Ceramics, Vol. 3), A.H. Hever and L.W. Hobbs, eds., American Ceramics Society, Columbus, OH, 1981, pp. 241–253.

Sevcik, W.R.; and Stoner, B.L.: An Analytical Study of Thermal Barrier Coated First Stage Blades in a JT9D Engine. (PWA–5590; Pratt and Whitney Aircraft Group; NASA Contract NAS3–21033) NASA CR–135360, 1978.

Spores, R.; and Pfender, E.: Flow Structure of a Turbulent Plasma Jet. Thermal Spray: Technology, New Ideas and Processes; Proceedings of the National Thermal Spray Conference, ASM International, Metals Park, OH, 1989, pp. 85–92. 1989.

Stecura, S.: Optimization of the NiCrAl–Y/ZrO_2–Y_2O_3 Thermal Barrier System. NASA TM-86905, 1985.

Taylor, R.E.: A Description of the Thermophysical Properties Research Laboratories. Internal Report TPRL 181, Purdue University, West Lafayette, IN, 1982.

Thorpe, M.L.; and Kratochvil, W.R.: Inductive Heating for a New Type of Plasma. Thermal Spray: Technology, New Ideas and Processes; Proceedings of the National Thermal Spray Conference, ASM International, Metals Park, OH, 1989, pp. 9–18.

Van Roode, M.; and Beardsley, B.: Porosity Determination of Thermal Barrier Coatings. ASME Paper 88–GT–278, 1988.

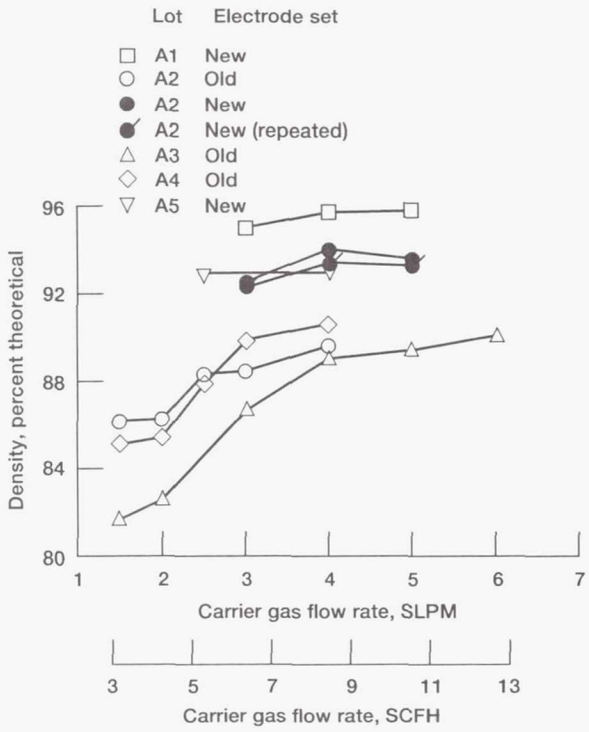

(a) Powder lots A1 to A5 sprayed at 40-kW power level. Arc gas, Ar-40% He; gas flow rate, 24 SLPM (51 SCFH).

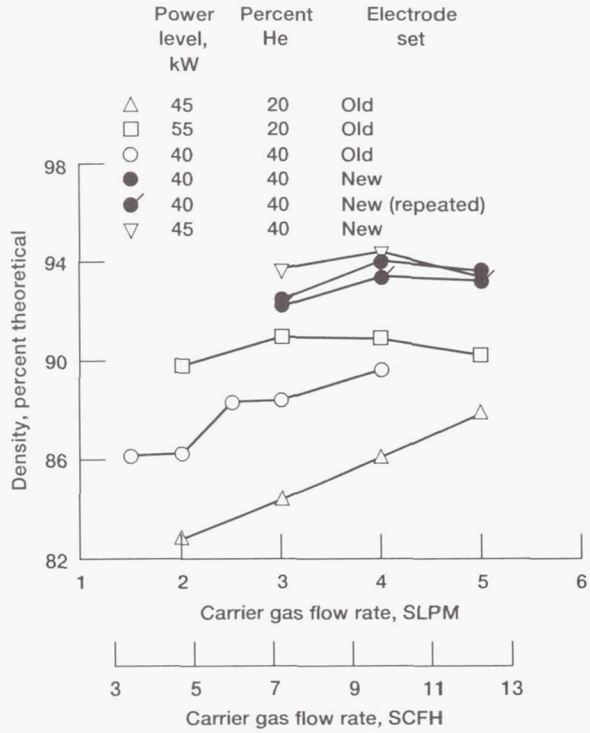

(b) Powder lot A2 sprayed at three combinations of power level and percent of He in the arc gas.

Figure 1.—Density versus powder carrier gas flow rate.

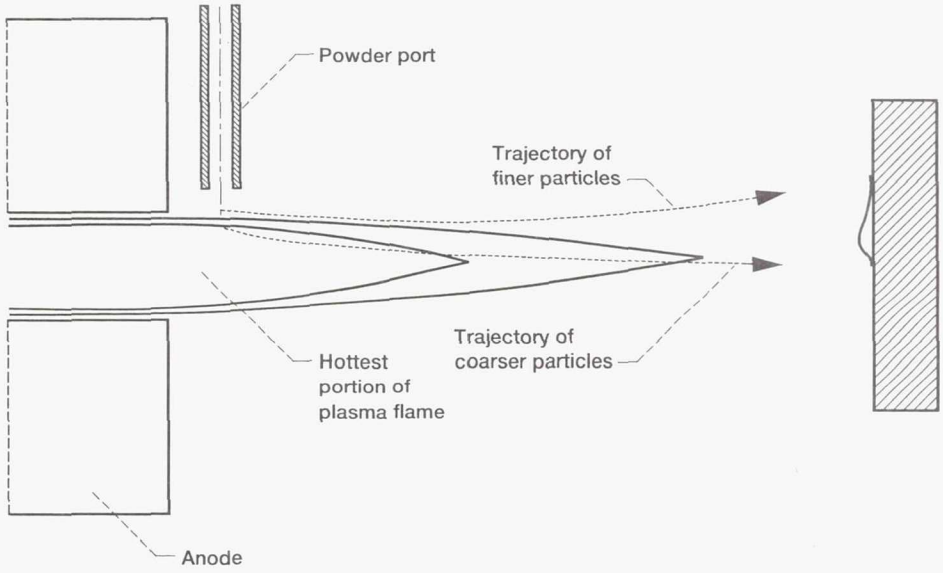

(a) Low flow rate.

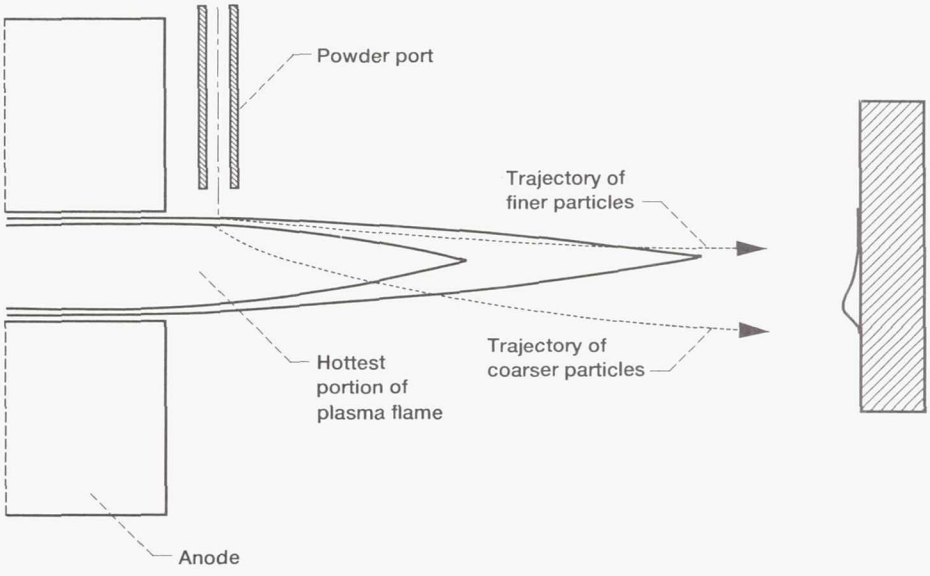

(b) High flow rate.

Figure 2.—Particle trajectories expected for low and high powder carrier gas flow rates.

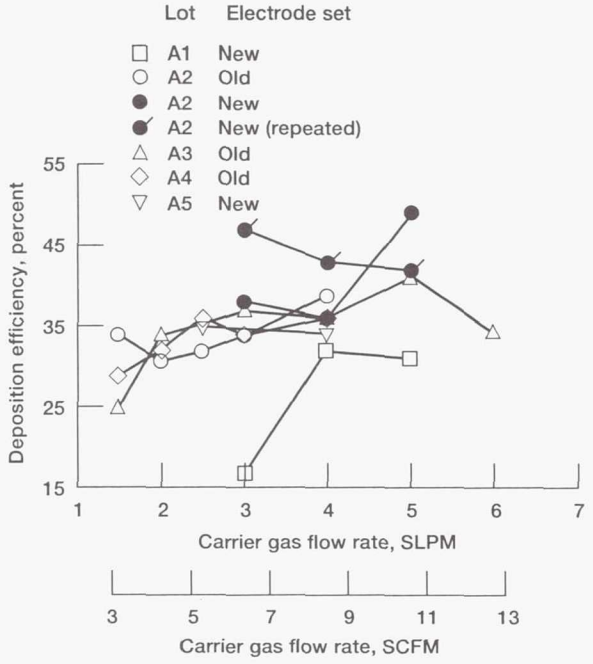

(a) Powder lots A1 to A5 sprayed at 40-kW power level. Arc gas, Ar-40% He; gas flow rate, 24 SLPM (51 SCFH).

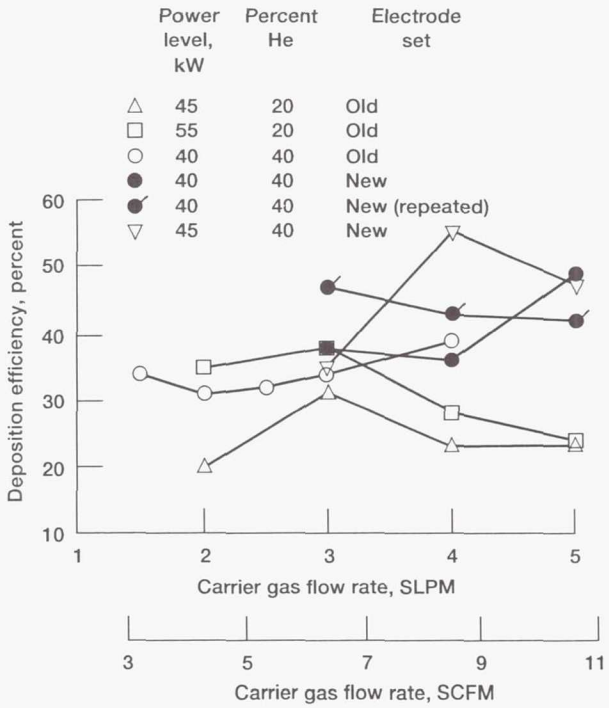

(b) Powder lot A2 sprayed at three combinations of power level and percent of He in the arc gas.

Figure 3.—Deposition efficiency versus powder carrier gas flow rate.

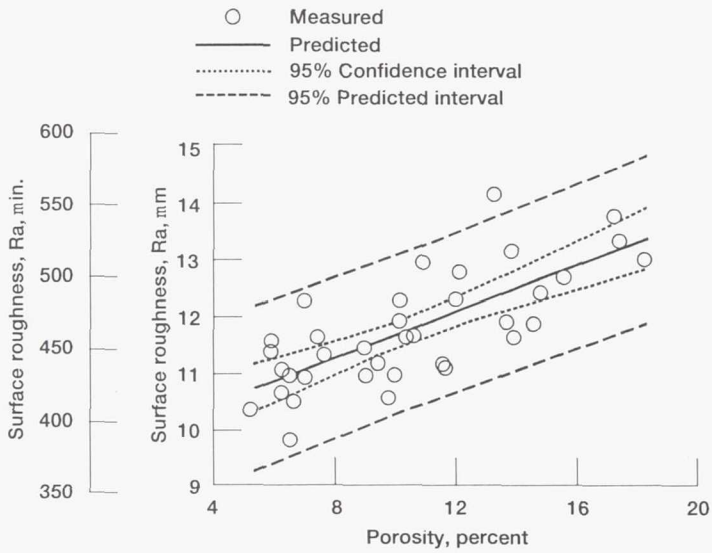

Figure 4.—Surface roughness versus porosity (correlation observed but measurement uncertainty precludes practical use).

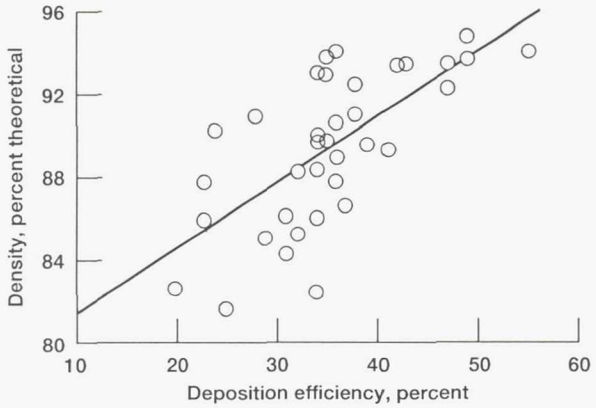

(a) Theoretical density versus deposition efficiency.

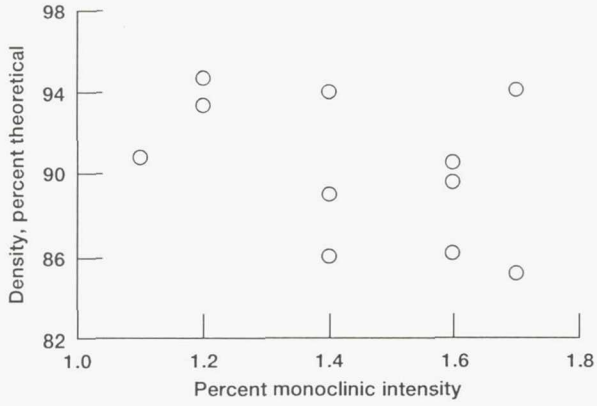

(b) Theoretical density versus percent monoclinic intensity.

Figure 5.—Relationship between percent theoretical density and deposition efficiency and percent monoclinic intensity.

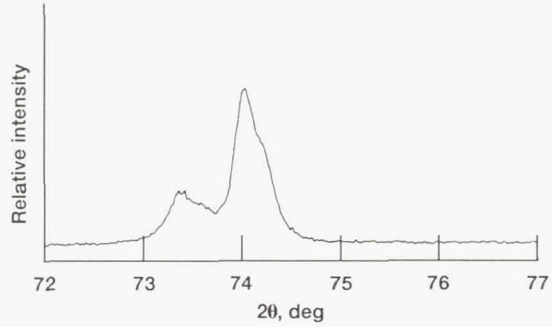

Figure 6.—X-ray diffraction pattern from (400) region for plasma-sprayed zirconia-yttria specimens. Note presence of t'-nontransformable tetragonal phase.

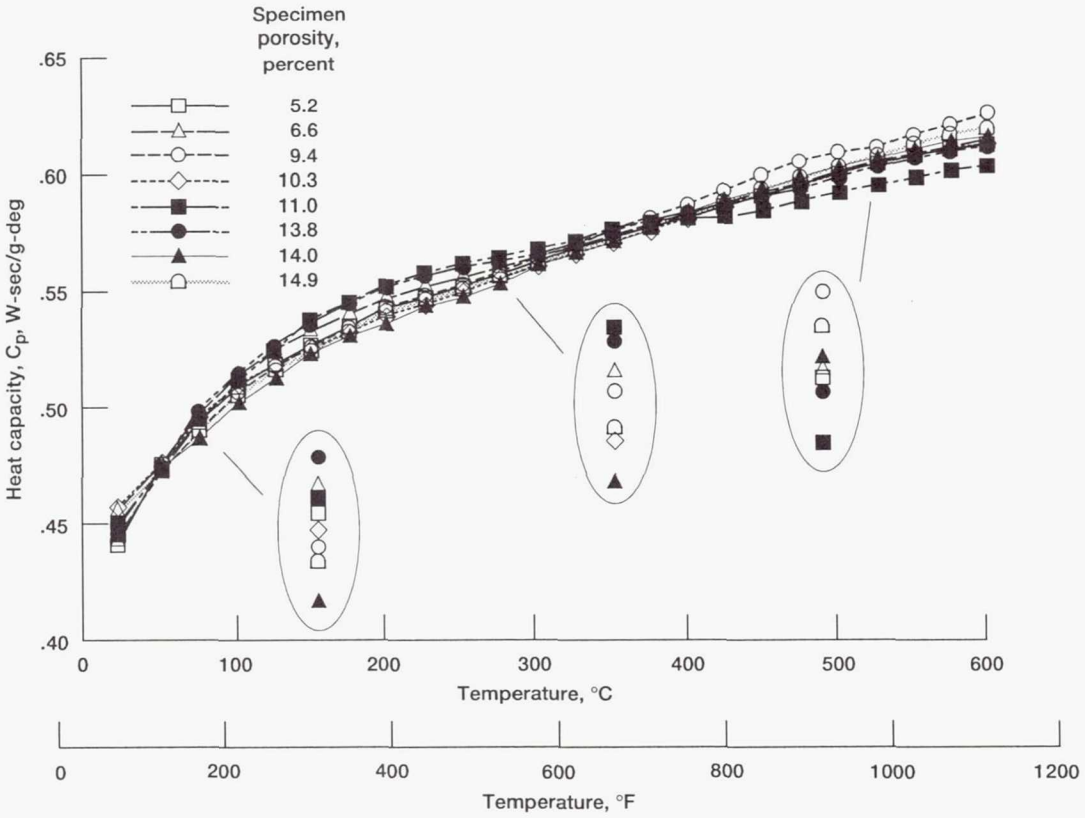

(a) Plasma-sprayed zirconia-yttria specimens (eight different porosities).

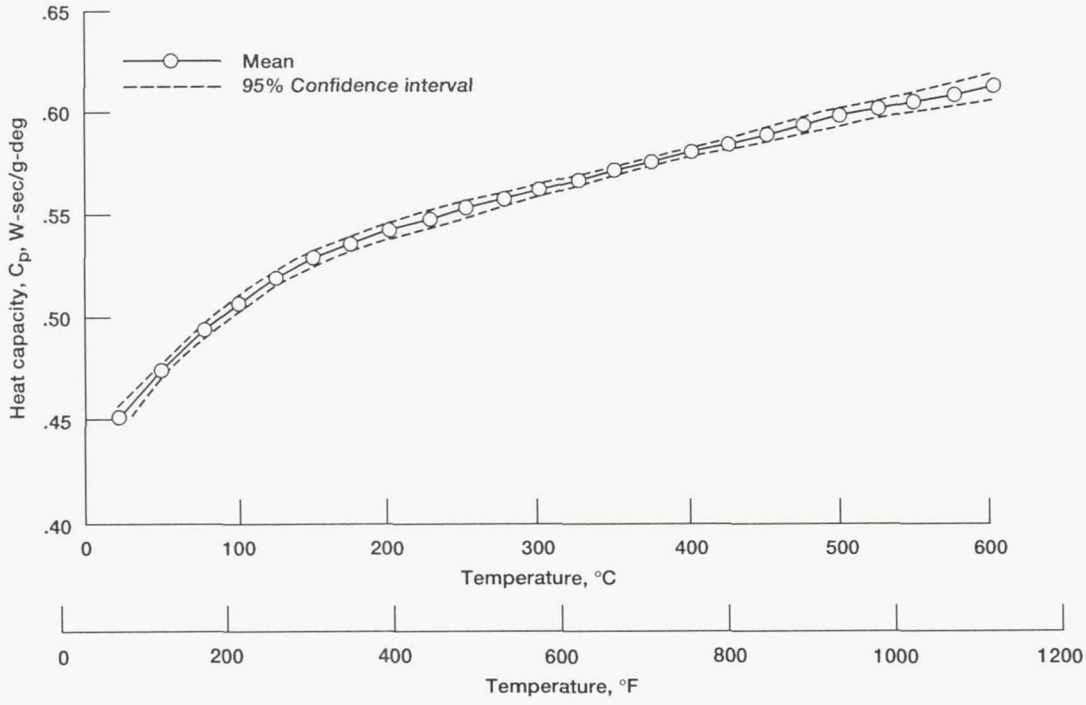

(b) Mean response from a regression fit.

Figure 7.—Measured heat capacities.

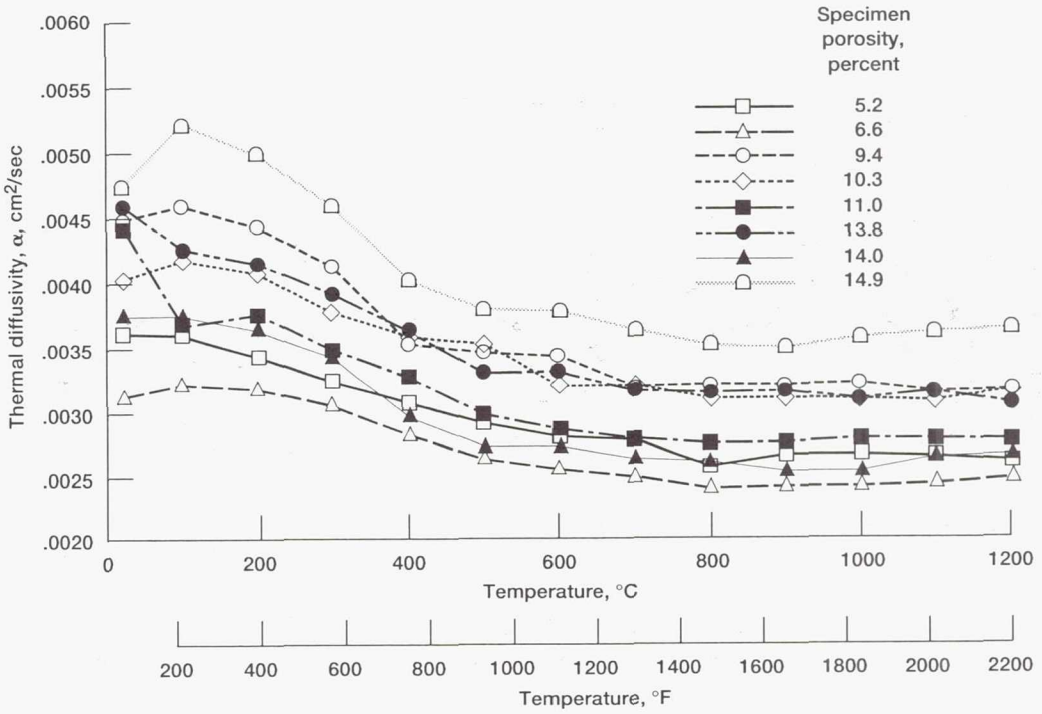

(a) On heating.

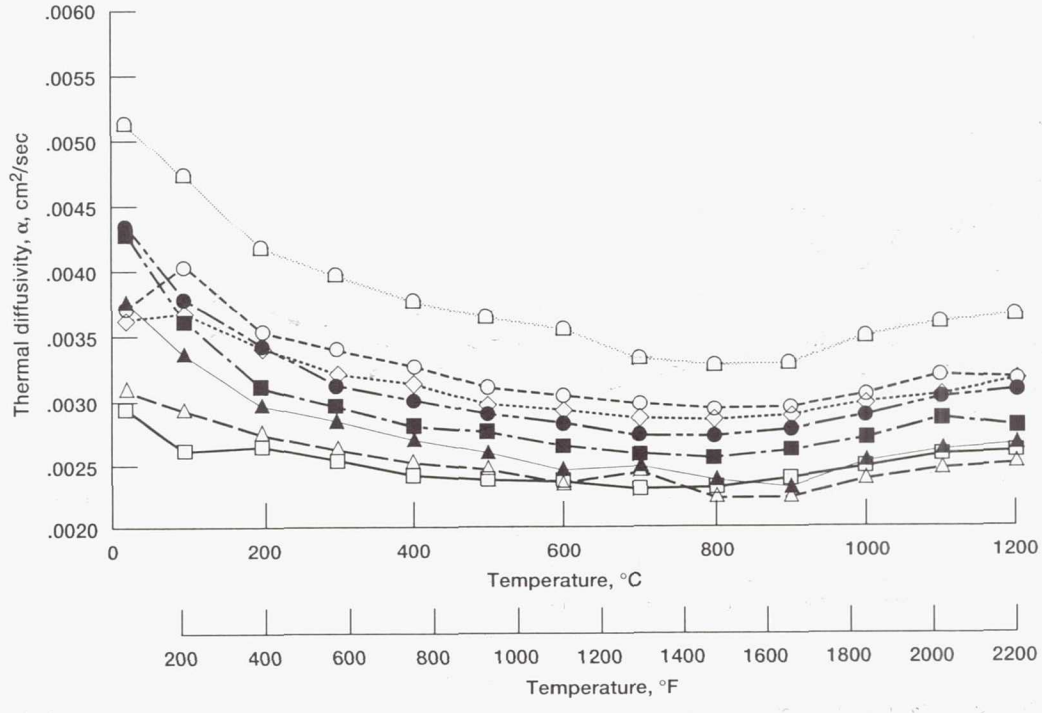

(b) On cooling.

Figure 8.—Measured thermal diffusivities for eight plasma-sprayed zirconia-yttria specimens.

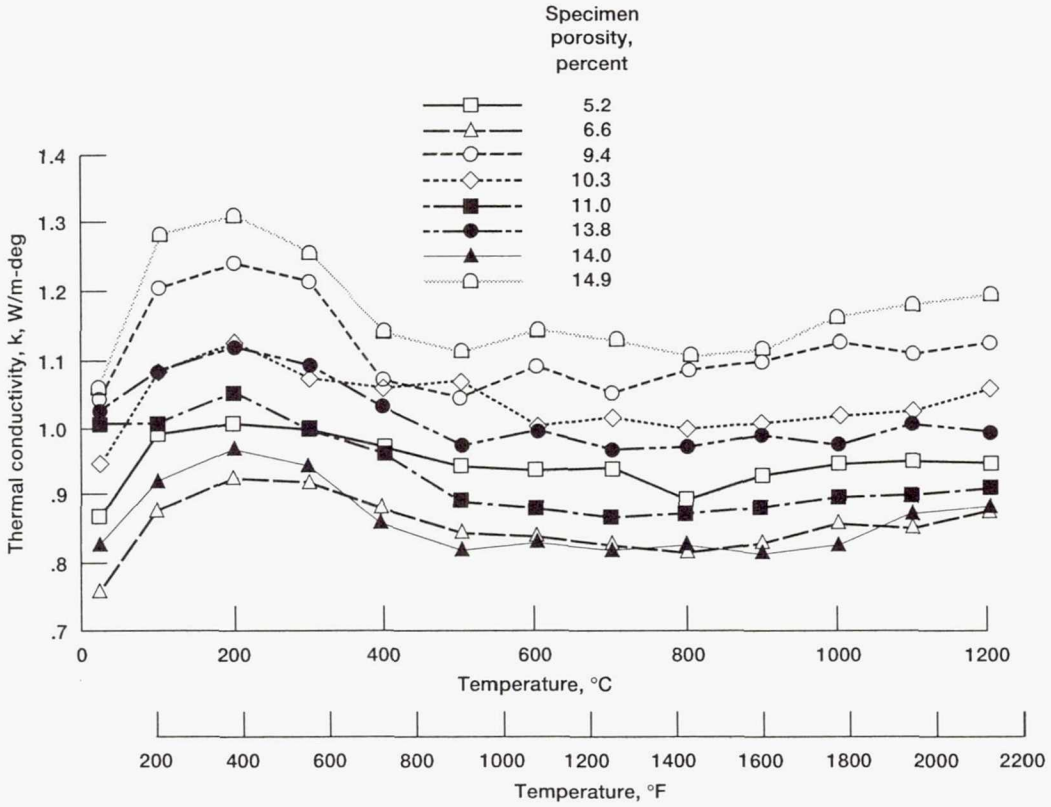

(a) On heating.

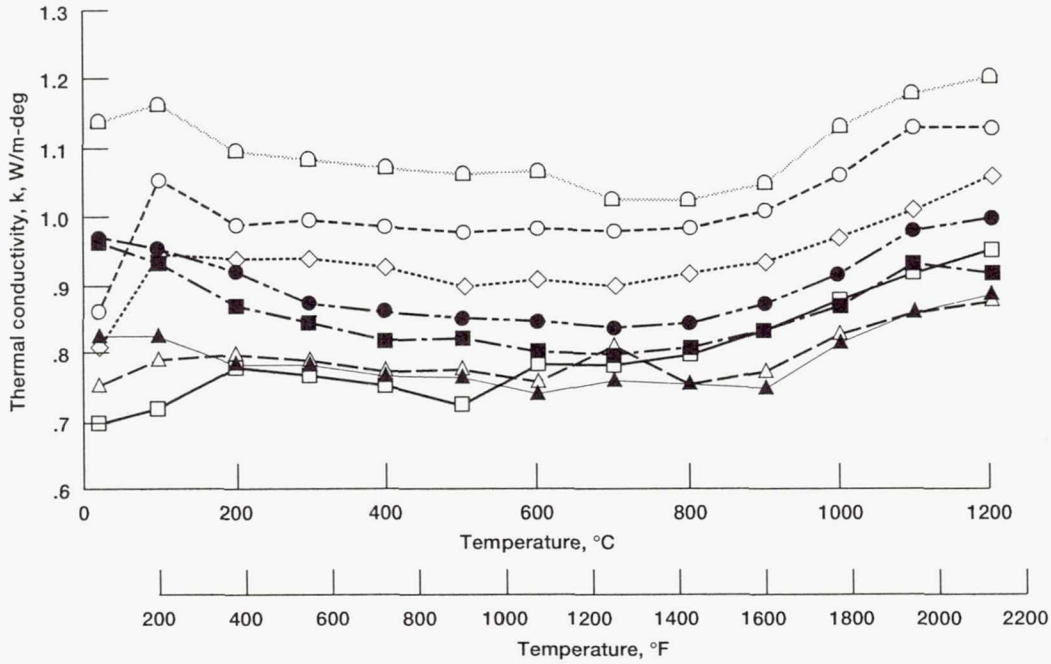

(b) On cooling.

Figure 9.—Calculated thermal conductivities for eight plasma-sprayed zirconia-yttria specimens. Measured diffusivities, measured/extrapolated heat capacities, and measured densities were used in calculations.

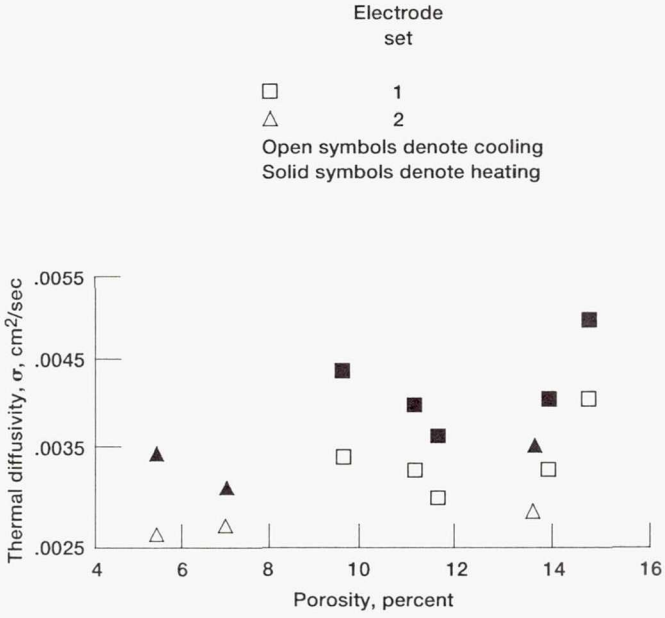

(a) Thermal diffusivity.

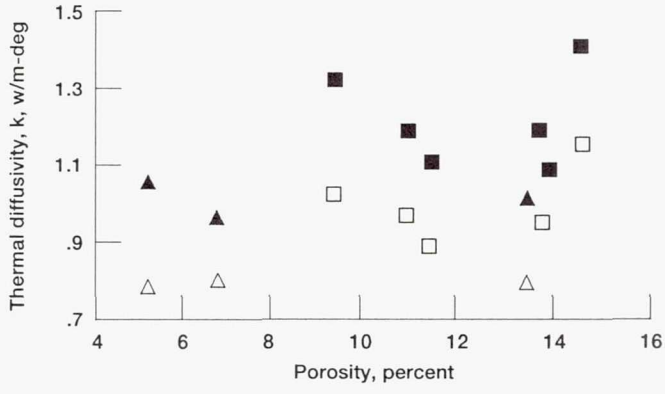

(b) Thermal conductivity.

Figure 10.—Thermal diffusivity and conductivity measured at 200 °C versus percent porosity and electron set.

6.6 Percent porosity

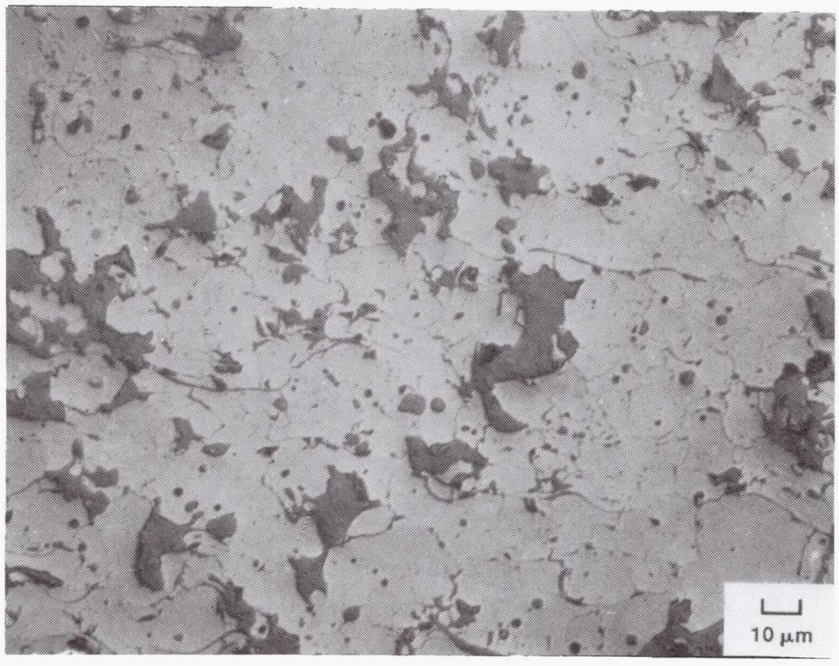

13.6 Percent porosity

Figure 11.—Cross sections of one of the more denser and one of the more porous of the thermal conductivity specimens. Note that the denser coating on the stainless steel substrates are highly cracked.

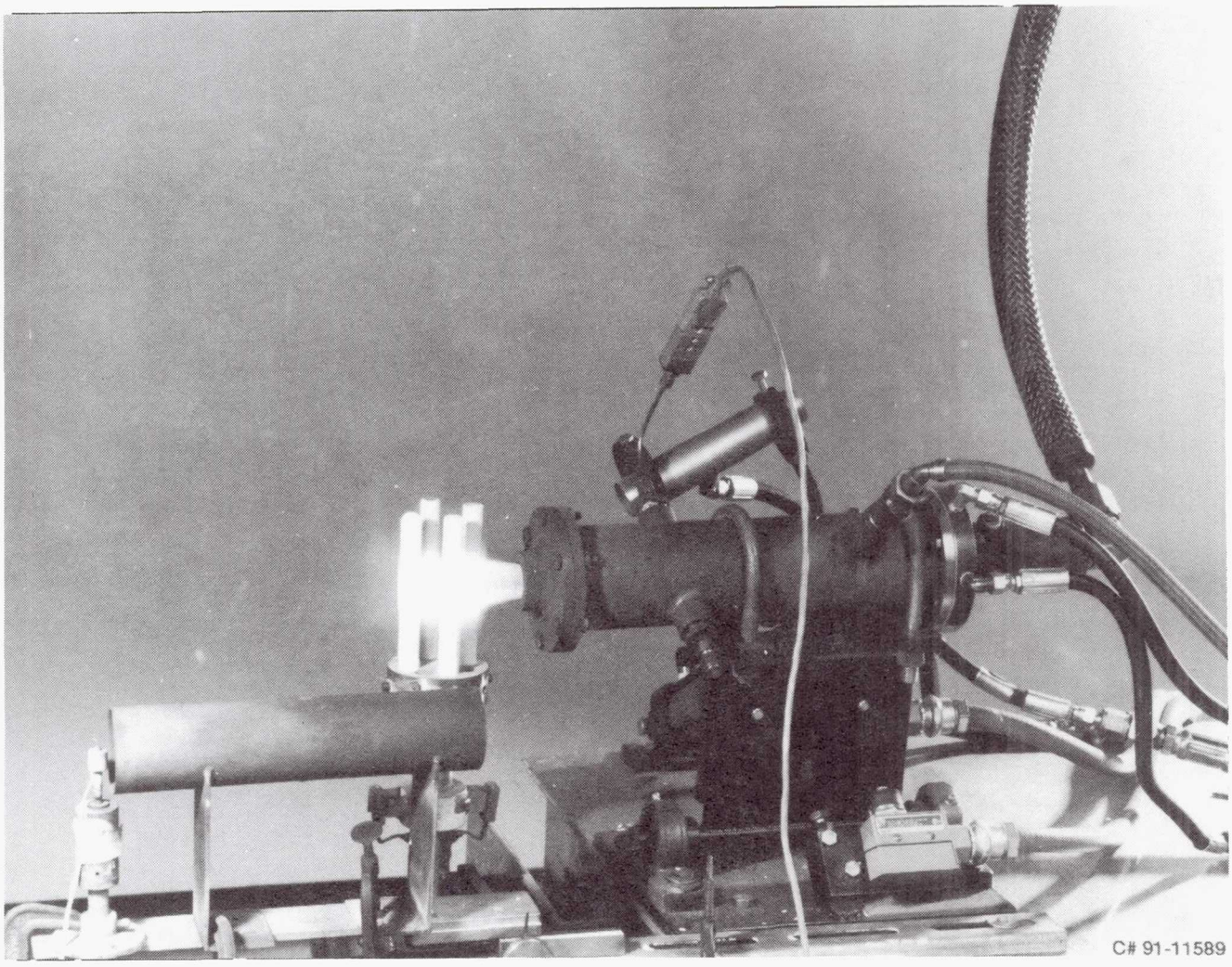

Figure 12.—Burner rig showing four-specimen rotating carousel.

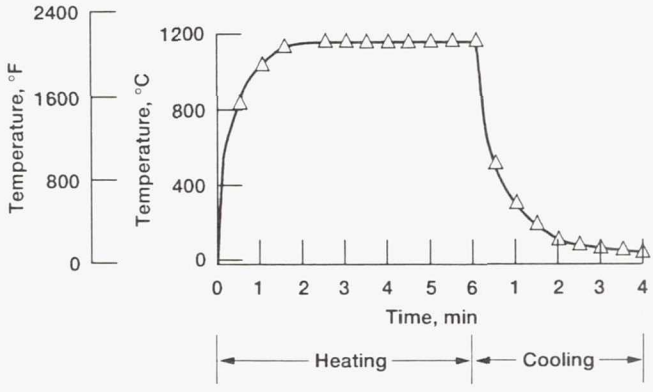

Figure 13.—Surface temperature of burner rig specimens during rig cycle.

(a) Rig and spray order not considered.

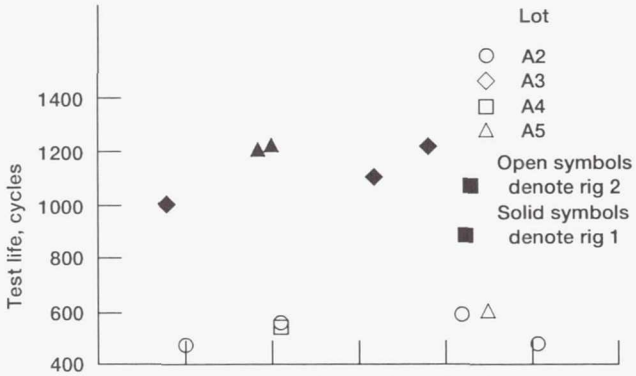

(b) Spray order 2 and rigs 1 and 2.

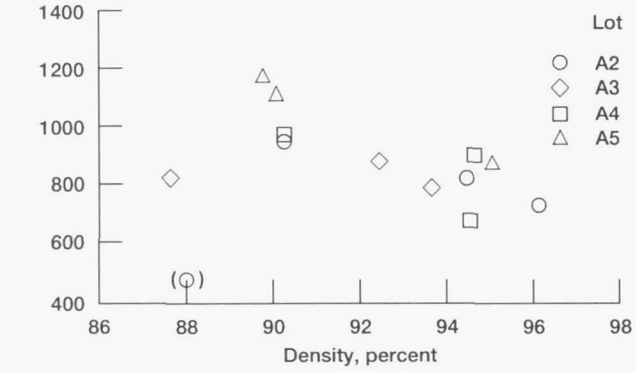

(c) Spray order 1 and rig 2.

Figure 14.—Burner rig life versus percent theoretical density. Temperature, 1150 °C (2100 °F).

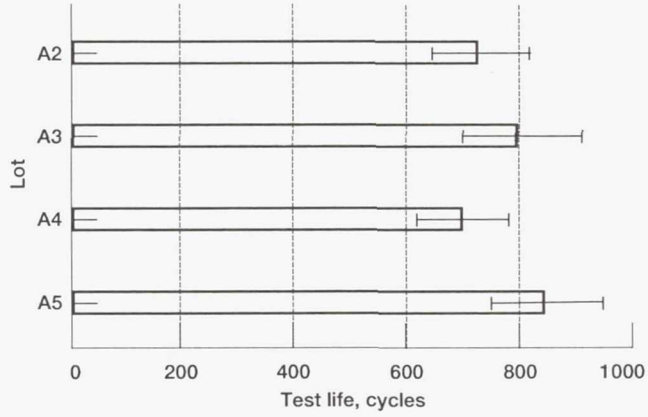

(a) Spray order 2 and rigs 1 and 2.

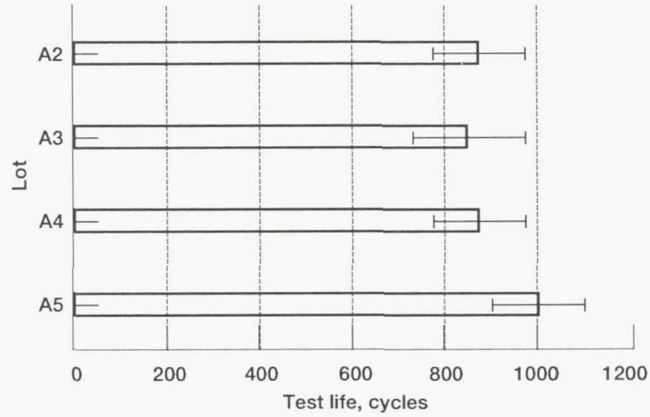

(b) Spray order 1 and rig 2.

Figure 15.—Coating response from analysis of covariance (ANCOVA) model. Means and 95-percent confidence intervals for zirconia-yttria lots A2 to A5.

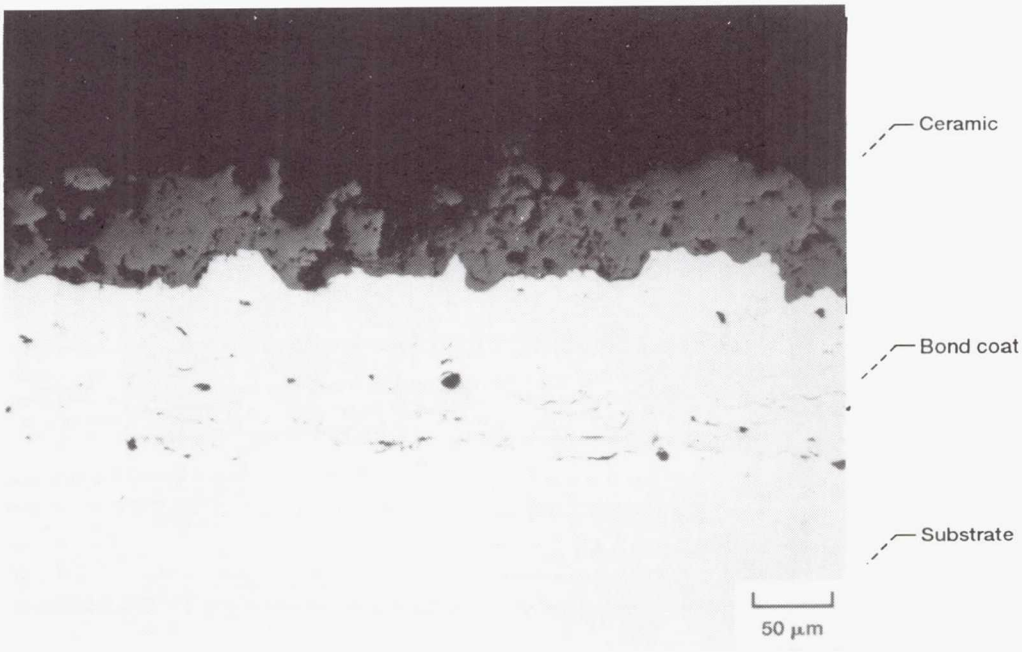

As-sprayed microstructure

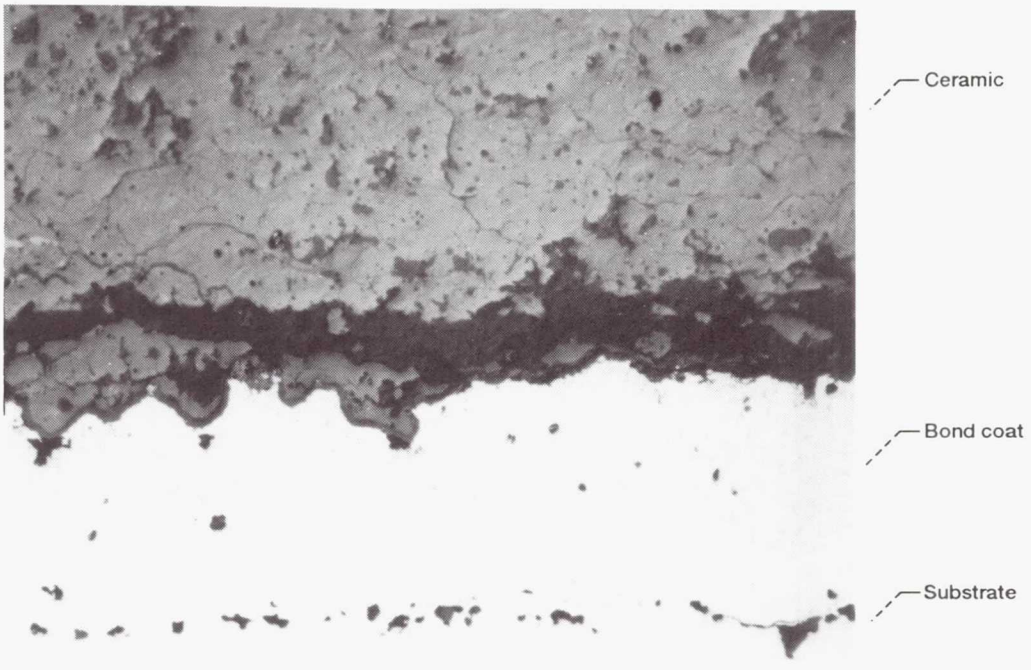

Hot zone after failure

(a) Spray parameter set, 40/40/1.5; spray order 1.

Figure 16.—Selected sections taken from near the base of test specimens for both as-sprayed microstructure and hot zone after failure. Bond coats are low-pressure, plasma-sprayed NiCrAlY; ceramic layers are from lot A_2.

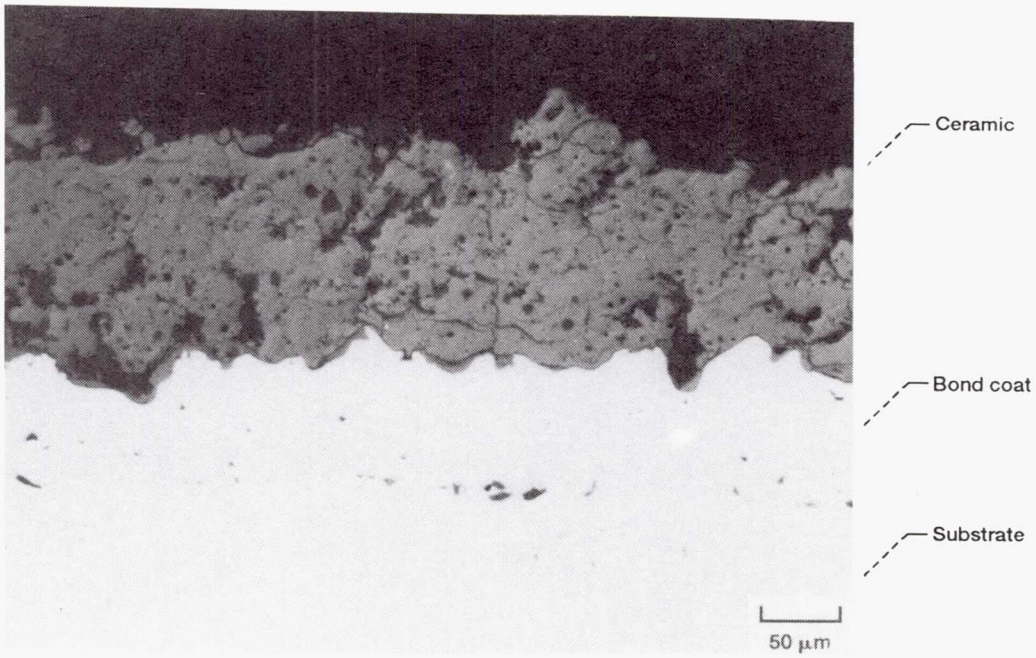

As-sprayed microstructure

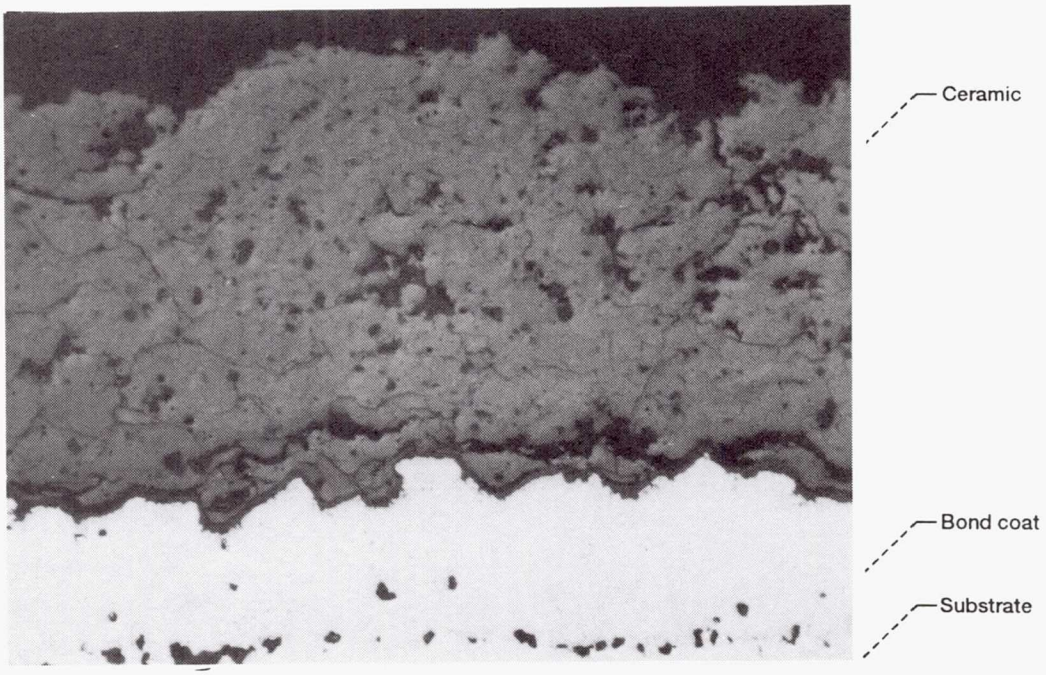

Hot zone after failure

(b) Spray parameter set, 40/40/1.5; spray order 2.

Figure 16.—Continued.

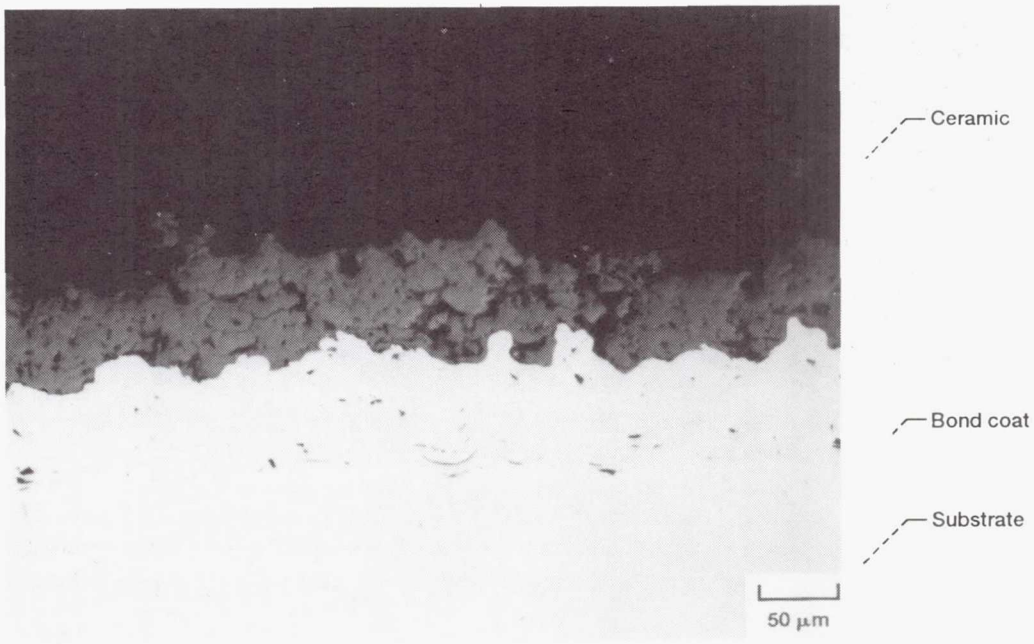

As-sprayed microstructure

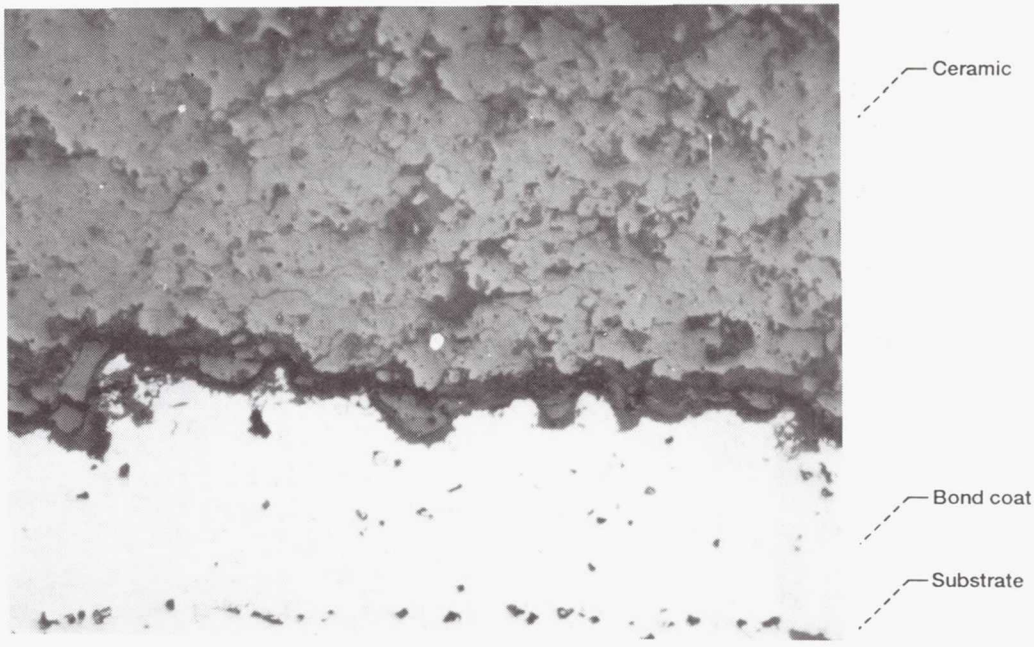

Hot zone after failure

(c) Spray parameter set, 45/20/4.5; spray order 1.

Figure 16.—Continued.

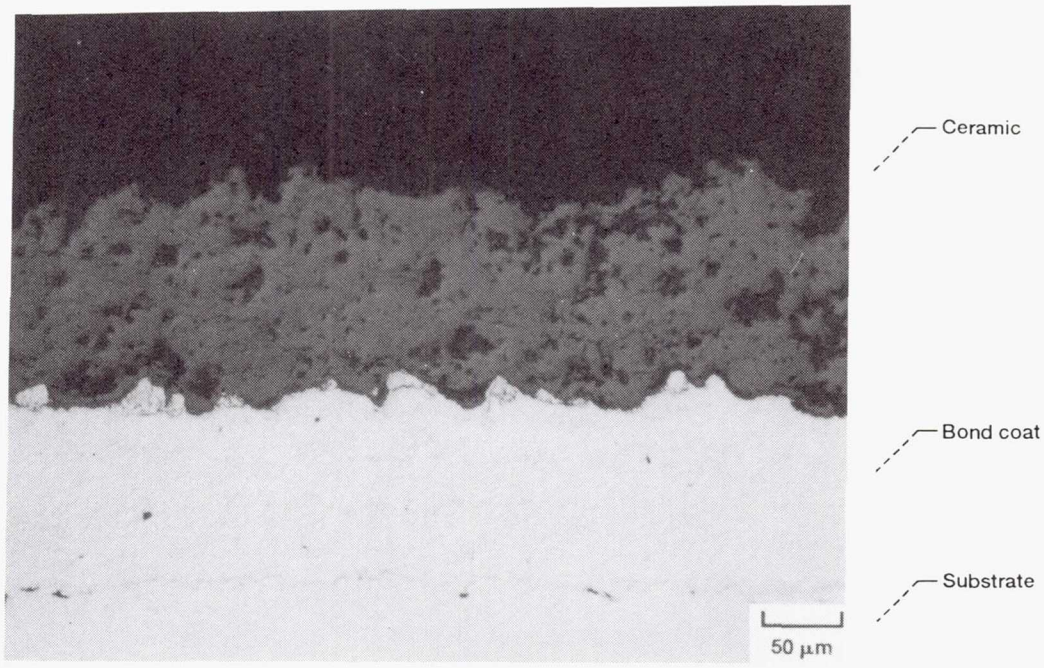

As-sprayed microstructure

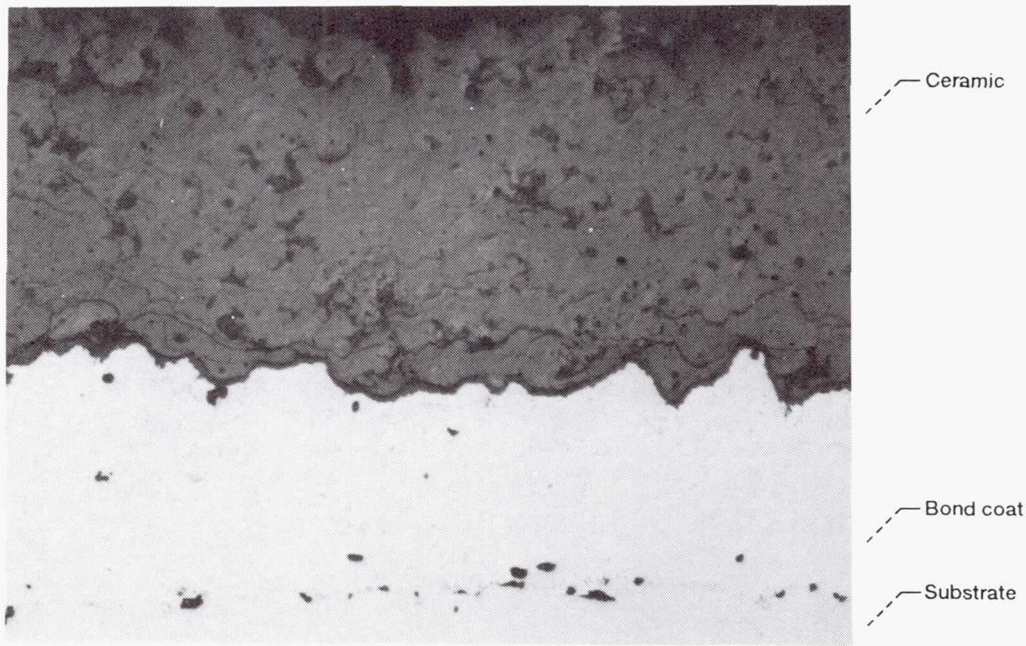

Hot zone after failure

(d) Spray parameter set, 45/20/4.5; spray order 2.

Figure 16.—Continued.

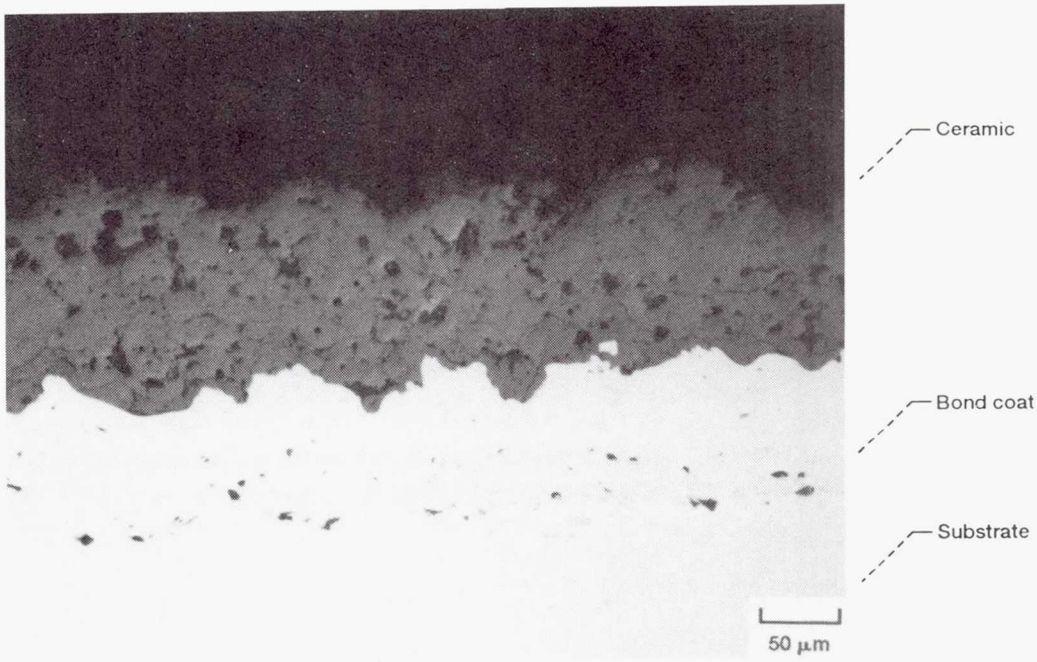

As-sprayed microstructure

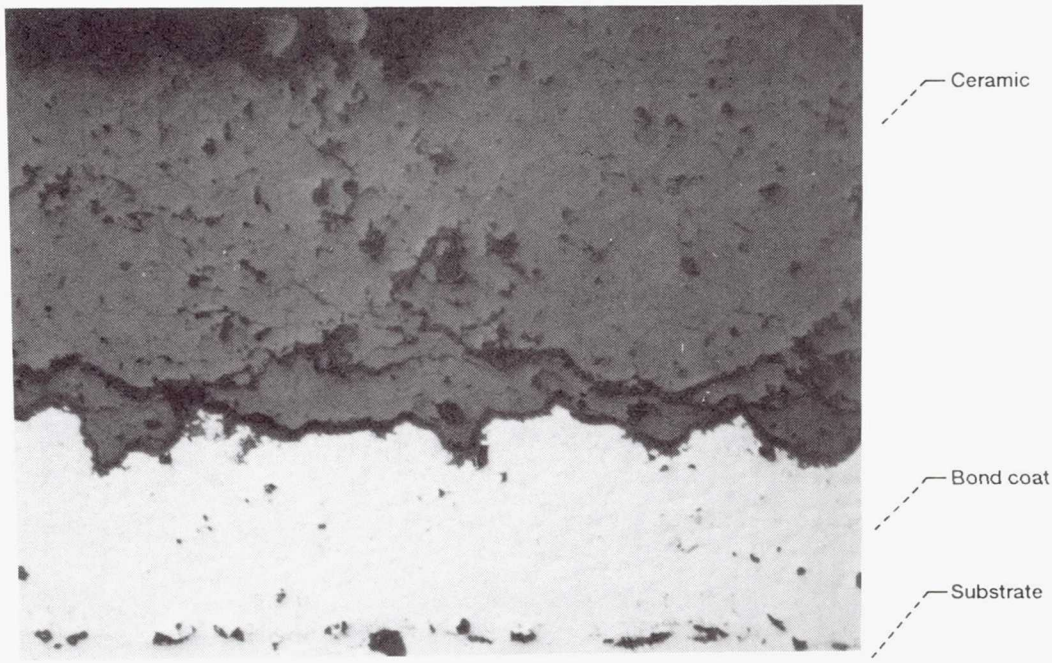

Hot zone after failure

(e) Spray parameter set, 55/20/4.5; spray order 2.

Figure 16.—Continued.

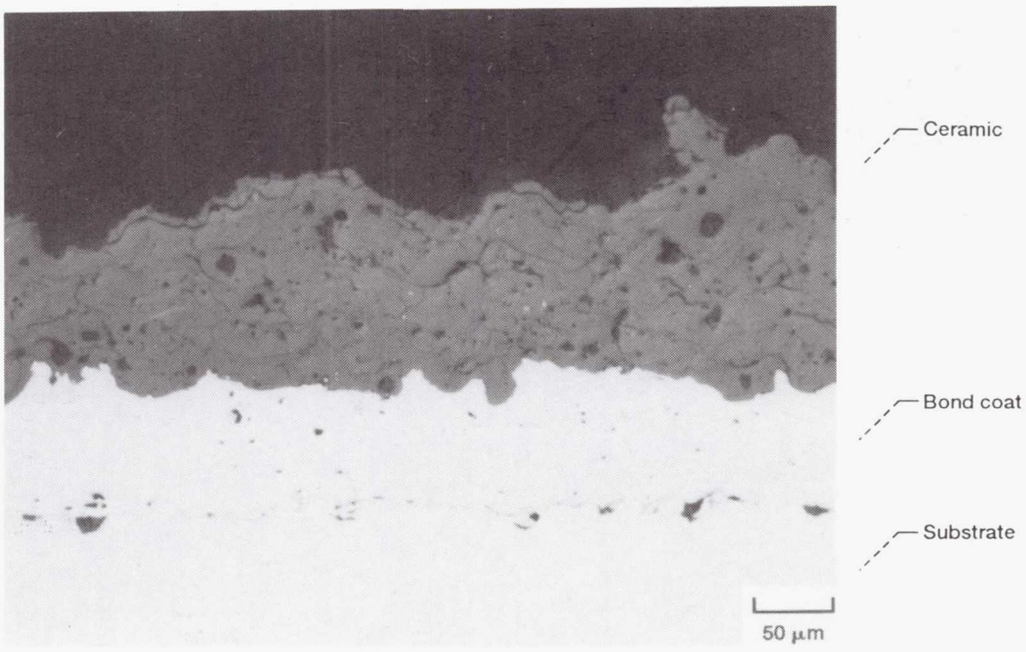

As-sprayed microstructure

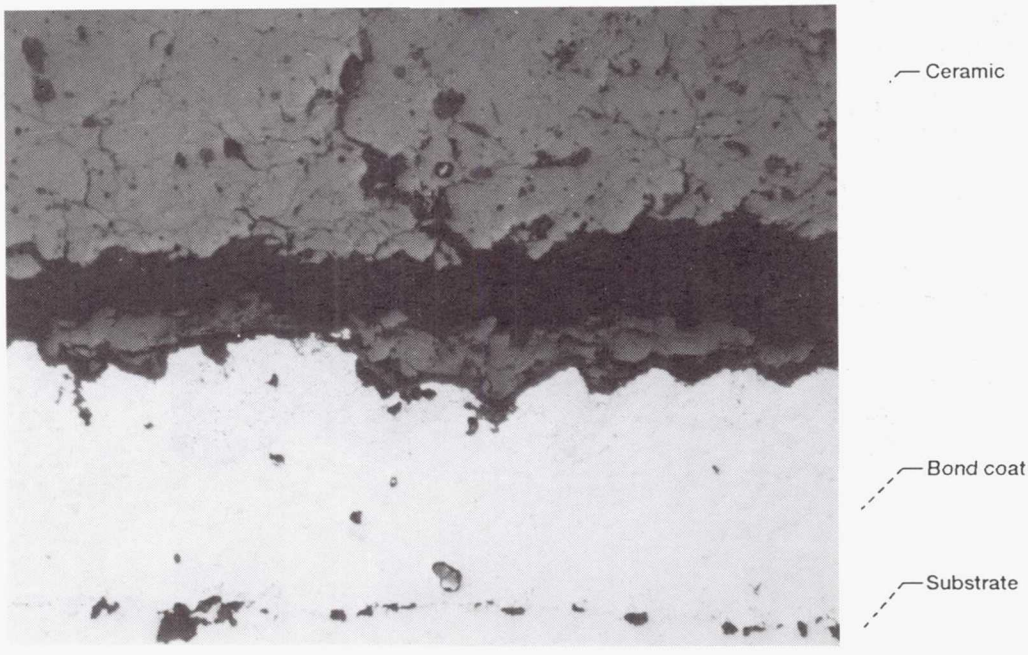

Hot zone after failure

(f) Spray parameter set, 40/40/4.5; spray order 1.

Figure 16.—Concluded.

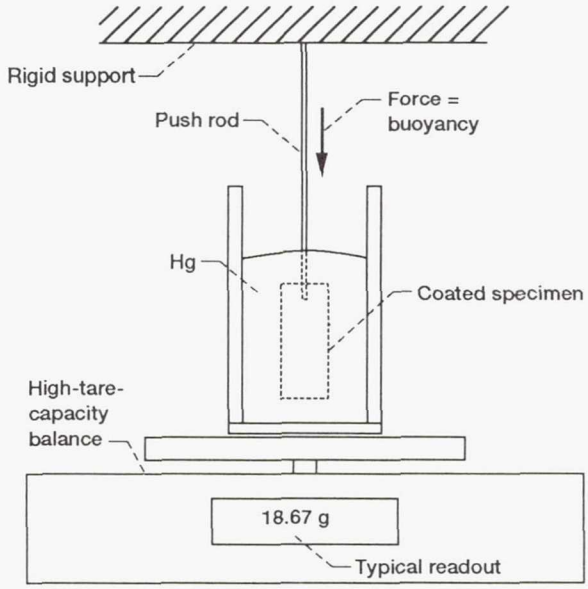

Figure 17.—Mercury Archimedes bulk density measurement apparatus.

REPORT DOCUMENTATION PAGE

Form Approved
OMB No. 0704-0188

1. AGENCY USE ONLY (Leave blank)	2. REPORT DATE	3. REPORT TYPE AND DATES COVERED
	February 1993	Technical Paper

4. TITLE AND SUBTITLE

Characterization and Durability Testing of Plasma-Sprayed Zirconia-Yttria and Hafnia-Yttria Thermal Barrier Coatings

Part I.—Effect of Spray Parameters on the Performance of Several Lots of Partially Stabilized Zirconia-Yttria Powder

5. FUNDING NUMBERS

WU-505-63-5A

6. AUTHOR(S)

Robert A. Miller, George W. Leissler, and J. Marcus Jobe

7. PERFORMING ORGANIZATION NAME(S) AND ADDRESS(ES)

National Aeronautics and Space Administration
Lewis Research Center
Cleveland, Ohio 44135-3191

8. PERFORMING ORGANIZATION REPORT NUMBER

E-7151

9. SPONSORING/MONITORING AGENCY NAMES(S) AND ADDRESS(ES)

National Aeronautics and Space Administration
Washington, D.C. 20546-0001

10. SPONSORING/MONITORING AGENCY REPORT NUMBER

NASA TP-3295

11. SUPPLEMENTARY NOTES

Robert A. Miller, NASA Lewis Research Center. George W. Leissler, Sverdrup Technology, Inc., 2001 Aerospace Parkway, Brook Park, Ohio 44142 (work funded by NASA Contract NAS3-25266). J. Marcus Jobe, Miami University, Oxford, Ohio 45056. Responsible person, Robert A. Miller, (216) 433-3298.

12a. DISTRIBUTION/AVAILABILITY STATEMENT

Unclassified - Unlimited
Subject Category 26

12b. DISTRIBUTION CODE

13. ABSTRACT ***(Maximum 200 words)***

This and the following report discuss initial experiments conducted on thermal barrier coatings prepared in the newly upgraded research plasma spray facility and the burner rig test facilities. Part I discusses experiments which establish the spray parameters for three baseline zirconia-yttria coatings. The quality of five similar coating lots was judged primarily by their response to burner rig exposure supplemented by data from other sources such as specimen characterizations and thermal diffusivity measurements. This study showed (after allowing for burner rig variability) that, although there appears to be an optimum density (i.e., optimum microstructure) for maximum burner rig life, the distribution tends to be rather broad about the maximum. In Part II, new hafnia-yttria-based coatings were evaluated against both baseline and alternate zirconia-yttria coatings. The hafnia-yttria coatings and the zirconia-yttria coatings that were prepared by an alternate powder vendor were very sensitive to plasma spray parameters, in that high-quality coatings were only obtained when certain parameters were employed. The reasons for this important observation are not understood. Also not understood is that the first of two replicate specimens sprayed for Part I consistently performed better than the second specimen. Subsequent experiments did not display this spray order effect, possibly because a chiller was installed in the torch cooling water circuit. Also, large changes in coating density were observed after switching to a new lot of electrodes. Analyses of these findings were made possible, in part, because of the development of a sensitive density measurement technique described herein in detail. The measured thermal diffusivities did not display the expected strong relationship with porosity. This surprising result was believed to have been caused by increased microcracking of the denser coatings on the stainless steel substrates.

14. SUBJECT TERMS

Thermal barrier coatings; Plasma spraying; Zirconia-yttria; Thermal diffusivity; Bulk density

15. NUMBER OF PAGES

36

16. PRICE CODE

A03

17. SECURITY CLASSIFICATION OF REPORT	18. SECURITY CLASSIFICATION OF THIS PAGE	19. SECURITY CLASSIFICATION OF ABSTRACT	20. LIMITATION OF ABSTRACT
Unclassified	Unclassified	Unclassified	

NSN 7540-01-280-5500

Standard Form 298 (Rev. 2-89)
Prescribed by ANSI Std. Z39-18

NASA-Langley, 1993